

# Synthetic polymers for Enhanced Oil Recovery; Mechanical degradation, and alleviation thereof

Experimental study across scales in pipes, chokes, and porous media of regular HPAM, HPAM-ATBS co-polymers, and TAPs

by

Siv Marie Åsen

Thesis submitted in fulfilment of  
the requirements for the degree of  
PHILOSOPHIAE DOCTOR  
(PhD)



Faculty of Science and Technology  
Department of Energy Resources  
2021

University of Stavanger  
NO-4036 Stavanger  
NORWAY  
[www.uis.no](http://www.uis.no)

©2021 Siv Marie Åsen

ISBN:978-82-8439-010-9

ISSN:1890-1387

PhD: Thesis UiS No. 592

---

## Acknowledgements

After reluctantly having agreed to peruse a PhD, there are some many people to be grateful to for finally being able to submit this work. It has been a bumpy, frustrating, and educational ride, which would not have been possible without the support and co-operation of Daniel Strand, Arne Stavland and Aksel Hiorth. Your efforts have been crucial and are appreciated beyond words.

The work and the “ride” have also been enriched by many interesting discussions with other colleagues at NORCE, and many of my thanks go to Olav Aursjø and Espen Jettestuen, for guiding me when I needed a peek into the pore scale world, and to Ingebret Fjelde and Nils Harald Giske for grounding my research in EOR (Enhanced Oil Recovery).

To Kristin Flornes, I am grateful for the proposition and facilitation, making it tempting for me to peruse this path, even though I have, on occasions, regretted it. Had it been a ski-trip, I would have returned to the cabin - or dug myself down.

To my former colleague Hilde Jonsbråten, my beautiful polymer princess, I am pining for all the good times we have had in the lab, and I miss you every day, except for the days when we visit each other at work.

Although during my scholarship, I have for the most part resided in my homely office and familiar laboratory at NORCE, I have been employed by the University of Stavanger (UiS), and my thankfulness also goes to many of my UiS-colleagues. I would like to thank Norbert Puttkamer for always being helpful when I felt lost in the administrative labyrinth. To Udo Zimmerman goes my appreciation for introducing me to geology by letting me join him and his students on a field trip to beautiful San Emiliano, in Spain. To Mahmoud Khalifeh goes my gratitude for encouraging me to really understand important parts of colloidal science. I also appreciated the interesting discussions with Rune Time regarding methods for visualizing polymer flow. And to Dimitri Shogin, I am thankful and inspired by his ambitious endeavour to voluntarily run a series of lectures on fluid dynamics of polymer solutions, and for always answering my questions on the subject.

---

I acknowledge the Research Council of Norway and the industry partners, ConocoPhillips Skandinavia AS, Aker BP ASA, Vår Energi AS, Equinor ASA, Neptune Energy Norge AS, Lundin Norway AS, Halliburton AS, Schlumberger Norge AS, and Wintershall DEA, of The National IOR Centre of Norway for support.

A special acknowledgment goes to Amare Mebratu, Halliburton for interesting discussions, his enthusiasm, and valuable contributions to the Large-Scale test constituting a major contribution to one of the papers.

The contributions of SNF, particularly Flavien Gathier, and BASF, specifically Roland Reichenbach-Klinke and Herbert Hommer, are also recognized and appreciated.

To Lynn P. Nygaard goes my gratitude for inspiration, motivation and comfort during a thesis writing course, which I wisely attended twice. Once at the start of my PhD-period and once when I was just about to start writing my “Kappe” (Cloak).

A special gratitude goes to friends Line Frøland and Helene Anda who made me laugh when all this got too much, and for lifting my spirits by being impressed by my work.

To my family, I thank you for your love, support and for always being there for me. My oldest daughter, Tone, I thank you for valuable feed-back, proof-reading and for involving me in your material science studies. My youngest daughter Jane, I thank you for interesting discussions, proof-reading and for following in my chemistry footsteps. My son, Jone, I thank you for your enthusiasm, for printing and designing flow geometries and for having your workweek in the lab with me. And my husband and best friend, Tore, I thank you wholeheartedly for technical support with the word template and other overwhelming inconvenience during my most desperate hour of technical despair.

I dedicate this work to my mother, Else Marie V. Åsen, father Svein Åsen and mother-in-law, Signe Bastiansen.

---

## Summary

This thesis and the related work concern synthetic polymers for enhanced oil recovery, their ability to reduce the mobility of the water phase during oil recovery, and their predisposition to mechanically break when subjected to certain flow conditions.

A major problem during water injection for pressure support and to push oil through the reservoir, is the adverse mobility ratio between water and oil. Water will usually have a lower viscosity than the oil, meaning it has less resistance to flow and moves more easily. It also flows more easily where the water saturation is high, giving a self-enforcing nature to viscous instabilities. In short, water will create low resistance flow paths for itself or flow in paths of low resistance, reaching the producer at a relatively early stage of injection and with large volumes of oil remaining to be produced. If the mobility difference between the injected phase and the oil is reduced, the oil will be displaced in a more piston-like manner, accelerating the oil production, increasing the volume of the reservoir contacted by the water, and delaying the water production.

The mobility difference can be improved by decreasing the mobility of the water phase through making it more viscous. This can be done by adding polymers. Polymer are large molecules composed of repeating chemical building blocks. The polymers used for Enhanced oil recovery (EOR) have molecular weight of millions of g/mol, so large that only a few hundred ppms added to the water is needed to increase the viscosity significantly.

Three categories of synthetic water-soluble polymers have been studied in this work, partly hydrolyzed polyacrylamide (HPAM), HPAM-ATBS co-polymers, and thermo-thickening associative polymers (TAPs). Their flow behaviour has been studied across scales in tubes, chokes, and porous media (unconsolidated sand, and Berea and Bentheimer sandstone).

HPAM is worldwide the most used polymer for Enhanced Oil Recovery (EOR), but there are several issues related to its use:

- Viscosity is reduced in saline water

- 
- It thickens in porous media at high flow rates typical for the injection zone, resulting in pressure build-up, poor injectivity or the creation of fractures
  - It is prone to mechanical degradation at harsh flow conditions, an effect amplified in saline water

Mechanical degradation is that the backbone of the polymer molecules ruptures, resulting in a polymer with a lower molecular weight and correspondingly lower viscosity, making the solution less effective in pushing oil to the producer.

HPAM-ATBS co-polymers are derivatives of HPAM that have been modified to be less influenced by salt in the mixing water. Due to a, on the molecular level, large appendix on the ATBS segments in the polymer, the polymer solutions' viscosity is not influenced as much by salt as HPAM. This is because it, due to steric hindrance, remains expanded. Also, since it remains expanded, mechanical degradation will not increase with salinity of the mixing water.

TAPs are polymers mainly composed of HPAM and (H)PAM-ATBS (or other water-soluble polymers), that have been modified to be triggered by heat. At a certain temperature, segments of them will become hydrophobic and through hydrophobic interactions, they bind weakly to each other creating a reversible weakly cross-linked gel with increased resistance to flow. This effect is, in addition to being triggered by heat, also enhanced by salt and porous media flow, and is strongly shear-thinning. This makes TAPs very promising for EOR operations as they will have low resistance to flow at the high injection rates at the often cooled down injection zone, and high resistance to flow at the low rates of the warmer main part of the reservoir. As their thickening does not only rely on the molecular weight, lower molecular weight polymers can be used. Lower molecular weight polymers are less predisposed to mechanical degradation and injectivity problems.

In this work we have studied mobility and mechanical degradation of HPAM and HPAM-ATBS in porous media over two order of magnitude of flow rates as a function of length,  $L$ . We confirmed that HPAM's degradation is more salt dependent than HPAM-ATBS. It was also found that at velocities above the critical velocity for onset of degradation, degradation continues for at least 20

---

meters, and following the initial inlet degradation, the viscosity declines with  $L^x$ , where  $x = -0.1$  for high molecular weight HPAM in synthetic seawater. This degradation is associated with unrealistically large pressure gradients which will not occur in the main part of the reservoir. It was also confirmed experimentally, that when velocity declining as a function of length, degradation will be limited to the highest velocities.

Degradation experiments in cylindrical pipes of different dimensions also confirmed that salt accelerates mechanical degradation more for HPAM than for HPAM-ATBS, and that high molecular weight polymers are more prone to mechanical degradation than low molecular weight. It was also found that mechanical degradation scales with shear rate, and not with pressure drop, velocity or Reynolds number, and that even at turbulent flow, degradation will not increase with length of the tube. That is, degradation seems to be limited to the inlet of the flow constriction. Since pressure drop itself does not harm the polymer, polymer solutions can be choked (have its pressure reduced) as long as the shear rate is kept below a critical value. Three methods for choking with acceptable degradation were experimentally identified: 1) Take the pressure drop out over a longer distance (long tube), 2) Use several chokes in series, each below a critical pressure drop or 3) Choke concentrated solution.

Testing of TAPs with increasing content of the temperature-triggered segment in different porous media confirmed the assumption that a critical concentration of either polymer or the active segments are needed to achieve thermo-thickening. It was also confirmed that below their critical temperature, their flow behaviour is like the unmodified mother polymer, and this is also (for the most part) the case for bulk flow (tube flow), even at elevated temperature. These experiments were not performed to study mechanical degradation and were run below the critical shear rate for degradation, but their high flow rate behaviour will most likely be that of a medium molecular weight PAM-ATBS co-polymer, as that is the main constituent of these polymers. The experiments revealed that within the limited diversity of these tests, type of porous media did not significantly influence the thermo-thickening. At high salinity, homogenous and stable thermo-thickening was achieved in a 76 cm long sand-pack, but the build-up of resistance to flow was slow, and for the weaker systems tested (lower associative content or salinity), resistance to flow collapsed at very low velocities. These systems still show great promise

---

regarding EOR, but a better understanding of the mechanisms guiding their behaviour is needed for optimum design for specific field conditions.

---

## Table of Contents

Acknowledgements .....	i
Summary.....	iii
1 Introduction .....	1
1.1 Motivation .....	1
1.2 Water based Enhanced Oil Recovery .....	3
1.3 Polymer flooding for Enhanced Oil Recovery .....	5
1.3.1 Polymers' effect on Mobility ratio.....	5
1.3.2 Field considerations and challenges.....	8
1.4 Overview of the papers and challenges addressed.....	9
2 Theoretical framework, concepts, and definitions.....	11
2.1 Polymers' composition, configuration, and dimensions.....	11
2.1.1 Molecular structure of selected EOR polymers .....	18
2.2 Bulk rheology.....	25
2.2.1 Laminar flow in circular tubes .....	33
2.2.2 Turbulent flow in large pipes .....	34
2.3 Porous media behaviour of polymer solutions.....	35
2.3.1 Mobility reduction.....	35
2.3.2 Porous media rheology.....	37
3 Experimental; methods and materials .....	47
3.1 Water composition .....	48
3.2 Polymer solutions.....	52
3.3 Core mounting and sand packing .....	56
3.4 Flooding rigs and set-ups.....	61
4 Results: Key findings and Discussion.....	67
5 Further work .....	75
6 Concluding remarks .....	78
7 References .....	81
PAPERS .....	88

---

## List of Figures

Figure 1 Development in Brent spot oil price (\$/barrel) from January 2011 to January 2021. From <a href="https://bors.e24.no/#!/instrument/C:PBROUSDBR%5CSP.IDC">https://bors.e24.no/#!/instrument/C:PBROUSDBR%5CSP.IDC</a> ENE viewed 15.01.2021.....	2
Figure 2 Generic relative permeability curve. ....	6
Figure 3 Fractional flow of water as a function of oil saturation for different mobility ratios. ....	7
Figure 4 Illustrating different types of polymer: 1) Homopolymer 2) Alternating copolymer 3) random copolymer 4) block copolymer 5) random terpolymer 6) graft copolymer. All illustrations, except 5 and 1, are bipolymers (two different monomer units). All except 6, are linear polymers. The figure is inspired by figure on <a href="https://en.wikipedia.org/wiki/Copolymer">https://en.wikipedia.org/wiki/Copolymer</a> (viewed 20210108), original image by en>User:V8rik. ....	12
Figure 5 Illustrating how the length of a monomer unit is calculated. ....	13
Figure 6 Molecule building set.....	15
Figure 7 General chemical structure of PAM ( $x=0$ $y=0$ ), HPAM ( $y=0$ ) and ATBS-type ( $y>0$ ). ....	19
Figure 8 Molecular structure of PEO and PNIPAM.....	23
Figure 9 A simple model illustrating the dimensions of the polymer with grafting density 0.17% described by Hourdet et al. (1994). Scale ~1:50 000. The purple circle has the radius of the calculated random coil of the backbone. The blue line represents the contour length of the acrylic acid backbone and the red lines represents the contour length of the PEO-side chains. The thicknesses of the lines are not to scale. ....	25
Figure 10 The rod-climbing Weissenberg-effect.....	28
Figure 11 Shear-thinning models and measured viscosity. ....	31
Figure 12 The relative viscosity (closed black symbols) is the shear-thinning viscosity of the fresh polymer solution plotted against the shear rate in the rheometer. RF (open black symbols) is the mobility reduction in the porous media as a function of the porous media shear rate. The remaining viscosity (normalized) of the effluent (red open symbols) is plotted against the porous media shear	

---

	rate at which the polymer solution was degraded. The polymer solution is 1000 ppm high molecular weight HPAM in 0.5%NaCl.....	39
Figure 13	The random coil (red dot), its contour length (red line) and model pore body and pore throat to scale. The width of the line is <b>not</b> to scale, and that conformation (fully stretched) not realistic (very improbable).....	42
Figure 14	Vacuum-filtration system.....	50
Figure 15	Calculated viscosity as a function of temperature for the salt waters. ....	52
Figure 16	Cores being drilled out of a 40cmx40cmx30 cm block by Ronny Håland, UTC. (Photo: Ronny Håland). ....	57
Figure 17	The pieces of the core holder. ....	59
Figure 18	Flooding rig for studying length effects. ....	62
Figure 19	Sketch of the experimental set-up/flooding rig with 3 cores and capillary tubed (CT) in series. The injection direction is from left to right, from low to high temperature. T1 was 20°C in all the experiments. T2 was 60°C and T3 was 80°C, in all but the first experiment (Experiment 1a), where they were 30°C and 60°C, respectively. ....	65
Figure 20	Sketch of the experimental set-up (flooding rig) with a 76 cm long sand pack in a steel cylinder used in Experiment 7 to 9. The dashed blue rectangle shows what is inside the heating cabinet. The blue lines show the capillary tubes (CT). ....	65
Figure 21	How the experimental set-up was used to test if introducing an extra entrance surface would influence our results.....	69
Figure 22	Modified flooding rigs. ....	70
Figure 23	Radial velocity gradient. ....	71

## List of Tables

Table 1	The recipes for the salt waters .....	49
Table 2	Polymer properties .....	52
Table 3	Calculated values of dimensions for the polymers used in this work at theta ( $\theta$ )-conditions. Note that the three last columns are	

---

calculated assuming that the monomer unit are the freely joint  
segments.....53

# **1 Introduction**

## **1.1 Motivation**

Although the relative amount of oil in the world's energy mix is slowly declining, the absolute consumption continues to rise (Ritchie, 2020). Access to affordable, transportable, and easy to use energy is important for the development of underdeveloped regions in the world.

In Norway, from which most of the petroleum production is exported and the oil industry is the largest source of income to society (country and citizens) (NorwegianPetroleum, 2019), oil production is declining from the larger fields, as many of them have entered their mature stage with oil being produced at high water cuts, i.e., high water to oil ratios (Askarinezhad et al., 2018; Skrettingland et al., 2014).

Figure 1 shows the development in oil price (\$/barrel) since 2011. The National IOR Centre of Norway was initiated in 2012. The oil prizes at the time would make profitable many projects which with today's prizes would be in deficit. With continued research on IOR (Improved Oil Recovery), hopefully the methods will be mature for the next upturn or developed to be profitable even in a low oil price scenario.



Figure 1 Development in Brent spot oil price (\$/barrel) from January 2011 to January 2021. From <https://bors.e24.no/#!/instrument/C:PBROUSDBR%5CSP.IDCENE> viewed 15.01.2021.

With current plans for production, over 50% of the oil resources on the Norwegian Continental shelf will be left in the ground (Åm et al., 2010). Fewer discoveries are made in developed areas, and if Norway is to maintain its oil production, Norway will have to open new areas for exploration and/or utilize the resources already discovered in areas with existing activity and infrastructure. The latter meaning: get more of the oil out of the fields already under production before they are abandoned. Many places in the world the “Challenging barrels” are targeted by what is called EOR, Enhanced Oil Recovery methods. The definition of EOR varies, but the simplest is maybe “injecting something, that is not already in the reservoir, into the reservoir, for the purpose of producing more oil”, very similar to the definition by Baviere (1991).

Enhanced oil recovery is also known as tertiary recovery. That is because it was originally seen as a way of extracting more oil after primary recovery (drainage by pressure depletion and pumping) and secondary recovery (pressure maintenance by water or gas injection). According to Baviere (1991), only about 15 % of the original oil in place is produced by primary recovery and roughly the same amount by secondary recovery, leaving 2/3 of OOIP (Original oil in place) to be targeted by EOR-methods. These numbers will of course be

strongly dependent on inherent reservoir properties (oil, water, rock, heterogeneities), and field developments.

In a study performed for the Norwegian petroleum directorate (NPD), Smalley et al. (2018) revealed that the technical EOR-potential of the Norwegian continental shelf (NCS) is 320 to 860 million standard cubic meters of oil. Methods including the use of polymers, will target around 50% of this oil. For reference the Johan Sverdrup field is, according to the Norwegian Petroleum Directorate's (NPD, 2019) Factpages, estimated to have 406 MSm<sup>3</sup> of recoverable oil.

Motivation for this work can also be found in Norwegian law, The petroleum act 's section 4-1: Prudent production, which states that:

*“Production of petroleum shall take place in such a manner that as much as possible of the petroleum in place in each individual petroleum deposit, or in several deposits in combination, will be produced. The production shall take place in accordance with prudent technical and sound economic principles and in such a manner that waste of petroleum or reservoir energy is avoided. The licensee shall carry out continuous evaluation of production strategy and technical solutions and shall take the necessary measures in order to achieve this.”*

Which means that for the stake holders to overhold this, a continued research revealing the best methods for achieving prudent production must be performed.

## **1.2 Water based Enhanced Oil Recovery**

When water is injected into an oil reservoir to maintain pressure and push oil to the producer, substantial amounts of oil will be left behind. On the microscopic level, oil droplets or immobile oil films will be capillary trapped in the pores (Emadi, 2012). Whether the oil is trapped as film or droplets, and the endpoint saturation will depend on the wettability. For a water-wet system the oil will be trapped as droplets in the larger pores, and the end-point oil saturation will be high and reached at an early stage. For an oil wet-system, much larger amounts of water are needed to reach end-point saturation, but the

amount of capillary trapped oil, as it constitutes a thin film on the surface of the pores, will be smaller compared to a water-wet case. The lowest residual saturation is reached for a mixed-wet case (Muggeridge et al., 2014). On the macroscopic level oil will be bypassed due to gravitational segregation, channelling of water in fractures or high permeability zones, or due to viscous fingering (“fingers” of water reaching the producer at a relatively early stage of injection, bypassing large volumes of the reservoir). In addition, oil can be trapped in compartments not connected with the rest of the reservoir (Muggeridge et al., 2014).

An EOR-process will increase the oil recovery by improving the microscopic or macroscopic sweep compared to what would be attained by injecting water (or by other secondary recovery method). This will accelerate the oil production so that more of the oil in place can be produced before the field, due to economic and technical limitations, must be abandoned. A detailed description of several EOR methods can be found in Baviere (1991) and Muggeridge et al. (2014) offer a description of the recovery mechanisms and limitations of various EOR-methods.

Microscopic sweep will be improved by reducing (e.g., surfactant or immiscible gas) or removing (e.g., miscible gas or solvent) the interfacial tension between the injected phase and the oil, or by favourable alteration of the wettability of the formation (e.g., by surfactant or optimizing the water chemistry). Optimizing the water chemistry will include the methods commonly referred to as “Smart water”, see e.g. Fathi et al. (2012) and low salinity water flooding, see e.g. Fjelde et al. (2012), Skrettingland et al. (2011). “Smart water” and low salinity flooding are two relatively new methods, both very sensitive to reservoir properties (rock, water, oil) (Austad et al., 2007; Fjelde et al., 2014; Piñerez T et al., 2016). Compaction of the reservoir, induced by the water chemistry, have also been suggested as a driver for improved oil recovery, but results diverge (Austad et al., 2007; Jensen et al., 2000; Sachdeva et al., 2020).

Improving macroscopic sweep is generally referred to as conformance control and will usually have the additional effect of also reducing water production (Borling et al., 1994). It can be achieved by in-depth water diversion or near well mechanical or chemical water shutoff (Askarinezhad et al., 2018;

Skrettingland et al., 2014) or by reducing the mobility ratio between in water phase and the oil phase. The latter can be done either by increasing the mobility of the oil phase or decreasing the mobility of the water phase, see Equation (2), below. Increasing the mobility of the oil can be attained by increasing the oil permeability or decreasing the viscosity of the oil. Decreasing the viscosity of the oil will be a mechanism of thermal recovery where viscosity of the oil is reduced by heating. Increasing the oil permeability will presumably be at play during favourable wettability alteration if it increases the relative permeability of oil. Decreasing the mobility of the water can be achieved by adding polymer to the water phase.

### **1.3 Polymer flooding for Enhanced Oil Recovery**

The oil left behind in un-swept areas due to heterogeneities in the reservoir and viscous fingering is the target for polymer-flooding. Certain polymers (due to elastic properties) can exert normal forces, affecting capillary trapped oil. However, if these effects are significant to reduce the residual oil saturation (improve the microscopic sweep) and lead to additional oil production beyond the effect expected from a pure viscosity increase, is still a matter of debate (Azad & Trivedi, 2019, 2020; Sheng et al., 2015).

Adding polymer to the injected water will both increase the viscosity and reduce the permeability; hence sweep is improved, water break through is delayed and oil production is accelerated.

#### **1.3.1 Polymers' effect on Mobility ratio**

The reason for the poor macroscopic sweep (both due to heterogeneities in the reservoir and viscous fingering) is simply the ease of which the different phases move in the reservoir, i.e., their mobility. How mobile a phase will be is dictated by the reservoir rock's permeability,  $k$  towards that phase at residual saturation of the other phase and the viscosity,  $\eta$  of the phase at prevailing conditions. The mobility,  $\lambda$  is defined as:

$$\lambda = \frac{k}{\eta}. \quad (1)$$

If the displacing phase (e.g., water or polymer solution) has a higher mobility, i.e., moves easier in the reservoir, than the displaced phase (oil), it will naturally reach the producer faster, and have contacted less of the reservoir volume, compared to when it is the displaced phase that has the higher mobility. Thus, the areal sweep will depend on the mobility ratio,  $\Psi$  the ratio of the mobility of the displacing and displaced phase. In the following the subscribed  $w$ ,  $o$  and  $p$  are used for water, oil, and polymer solution, respectively. In this work, the symbol  $\Psi$  is used for the mobility ratio instead of the more commonly used  $M$ , to avoid confusion with the molecular weight (introduced later).

$$\Psi = \frac{\lambda_w}{\lambda_o} = \frac{\eta_o k_w}{\eta_w k_o}. \quad (2)$$

Decreasing the mobility ratio will smooth the displacement front, whether the irregularity of the waterfront is caused by viscous fingering or heterogeneities, (that is water breaking through in high permeable zones). Viscous fingering is caused by the self-reinforcing nature of random instabilities, since it is easier for the water to move where water is already at a higher saturation, as the water permeability,  $k_w$  is strongly dependent on the water saturation,  $s_w$ , as illustrated in the generic relative permeability plot in Figure 2.

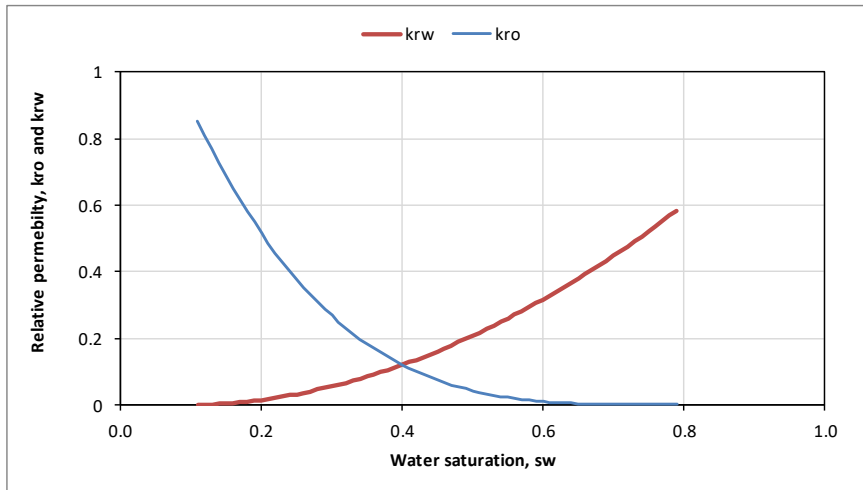


Figure 2 Generic relative permeability curve.

The impact of changing the mobility ratio on the oil recovery can be illustrated by calculating the fractional flow of water as a function of the saturation for

different mobility ratios. From Darcy's law for 1 dimensional, linear flow (e.g., a cylindrical core) the fractional flow of water,  $f_w$  will be given by:

$$f_w(S_w) \stackrel{\text{def}}{=} \frac{q_w}{q_o + q_w} = \frac{k_w(S_w)/\eta_w}{k_w(S_w)/\eta_w + k_o(S_w)/\eta_o}. \quad (3)$$

Using the synthetic relative permeabilities in Figure 2 and changing the water viscosity, the fractional flow of water as a function of oil saturation is shown in Figure 3. It is plotted against the oil saturation to illustrate that for the same fractional flow of water, the oil saturation in the core decreases with decreasing mobility ratio, showing that more of the oil has been produced for a lower water mobility, even for the simple case of a homogeneous linear core. For example, at a water cut,  $f_w$  of 80%, at lowest water viscosity, that is highest mobility ratio, the oil saturation left in the core is 58%. If the water viscosity is increased so that the mobility ratio is reduced to 0.7, the oil saturation at the same water cut will be 52% and will be reduced further to approximately 47% if the water viscosity is increased further to twice the viscosity of the oil, illustrating that for the same water cut, more of the oil will have been produced if the water viscosity is increased.

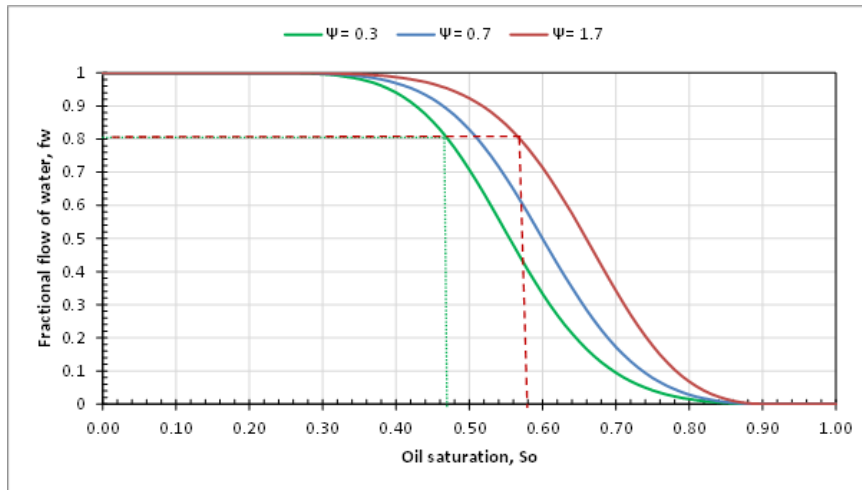


Figure 3 Fractional flow of water as a function of oil saturation for different mobility ratios.

Above, we have only looked at the viscosity change. The polymer will in most cases also change the permeability, due to adsorption and entrapment of

polymer molecules, so that  $k_p < k_w$ . This will further improve the mobility ratio compared to what is expected from only viscosity considerations.

The permeability reduction effect will also be maintained during the post polymer water flood, positively influencing the sweep. A detailed description of the mechanisms improving the sweep can be found in Sorbie (1991).

A water-soluble polymer will also impact the water permeability more than the oil permeability, an effect often taken advantage of in disproportional permeability reduction-operations (DPR) (Langaas & Stavland, 2020; Stavland & Nilsson, 2001).

### **1.3.2 *Field considerations and challenges***

Presently, polymer flooding is the most common water-based method for enhanced oil recovery (Sheng et al., 2015). The first pilot was performed as early as 1959 and indicated that the method would be profitable (Pye, 1964) and that the behaviour and results was as expected from the then prevailing theory (which is not much different from today's theory).

Literature reviews by Standnes and Skjevrak (2014) and Manrique et al. (2017) of polymer project have revealed that polymer projects are more efficient the earlier they are implemented. Although there may be good reasons for a preceding water flood (understanding the reservoir, calibrate models, establish base line, etc.), injecting polymer solutions in secondary mode will in terms of oil production and reduced water production usually be preferable. Accordingly, the abbreviation "EOR" is sometimes said, in a humoristic yet cautionary manner, to mean "Early Or Regret".

As mention, an additional advantage of polymer injection is the reduced/delayed water production, reducing the energy and effort needed to lift, separate, rinse and re-inject huge amounts of dirty, often radioactive water. On the other hand, there is also a substantial downside of potentially producing polymer solution, but if the project is successfully designed, this will happen at a later stage, when much more of the oil in place has been produced.

The literature reviews by Standnes and Skjevrak (2014), Manrique et al. (2017) and Sheng et al. (2015) aimed at identifying successes criteria and problematic

issues related to polymer flooding. Among the successes criteria are implementing the method early, large enough volumes injected, and maintaining high enough injection rates. To maintain high enough injection rate, a reduction in injected viscosity may be necessary, which will be a compromise between desired mobility reduction and reasonable injectivity. Among the problematic issues are premature production of polymer causing equipment failure and difficulties in separating oil and water, formation damage, injectivity loss, poor compatibility with mixing water (“make-up water”) or formation water, and loss of viscosity due to chemical, thermal, or mechanical degradation of the polymer. HPAM (hydrolyzed polyacrylamide) is the most used polymer for EOR and is, as will be discussed later, susceptible to mechanical degradation when subjected to shear and elongational stress which can occur in the porous media of the formation and in equipment. In porous media synthetic polymers are also prone to shear-thickening at high, near well velocity, which can result in injectivity problems.

#### **1.4 Overview of the papers and challenges addressed**

The key issues that are addressed in this work, are mechanical degradation in the porous media, specifically whether this will be a problem deep in the reservoir (Åsen et al., 2019), mechanical degradation in equipment, with focus on mitigation during choking (Stavland et al., 2021), and mitigation of injectivity issues and thereby mechanical degradation by the use of thermo-thickening associative polymers, which will also alleviate poor compatibility with salt containing make-up or formation water (Åsen et al., 2021) submitted 2021.

This work has of now resulted in 4 articles, 2 of them accepted for publication in journals, 1 submitted to a journal and 1 presented at a conference and published by SPE. The conference article covers essentially the same work as the first journal publication. Additionally, the work has been presented in talks and posters at conferences and workshops.

Conference paper:

Åsen, S. M., Stavland, A., Strand, D., & Hiorth, A. (2018, April). An experimental investigation of polymer mechanical degradation at cm and m

scale. In SPE Improved Oil Recovery Conference. Society of Petroleum Engineers. SPE-190225-MS (Åsen et al., 2018).

Journal paper 1:

Åsen, S. M., Stavland, A., Strand, D., & Hiorth, A. (2019). An Experimental Investigation of Polymer Mechanical Degradation at the Centimeter and Meter Scale. SPE Journal, 24(04), 1-700. SPE-190225-PA (Åsen et al., 2019).

Journal paper 2:

Stavland, A., Åsen, S. M., Mebratu, A., & Gathier, F. (2020). Scaling of Mechanical Degradation of EOR-polymers: From Field-Scale Chokes to Capillary Tubes. SPE Production & Operations. SPE-202478-PA (Stavland et al., 2021).

Journal paper 3 (submitted):

Åsen, S. M., Stavland, A., & Strand, D. (submitted, March 2021). Flow behavior of thermo-thickening associative polymers in porous media: Effects of associative content, salinity, time, velocity, and temperature. Submitted to Transport in Porous Media (Åsen et al., 2021).

Written works, in the form of essays, articles or reports, for the mandatory PhD-courses have also been produced:

- Field excursion report - The geology of the North Western part of Spain
- Science, philosophy of science, and philosophy in popular culture - with focus on science-fiction - Questions: How is science fiction and popular culture influence by science and is there a vice versa?
- Rheology of polymers for Enhanced Oil Recovery (EOR) in a societal perspective - Potential positive and negative impact in a Responsible Research and Innovation (RRI) perspective
- Hydrophobically associating water soluble polymers with enhanced thickening abilities - A literature review to support ongoing experimental investigation of porous media behavior of thermo-thickening polymers as a function of temperature, salinity, scale, associative content, (shear) rate and time

## **2 Theoretical framework, concepts, and definitions**

In the following, correlations and considerations describing the flow behaviour of polymer solutions in bulk and porous media, and how this relates to the mobility will be offered. To discuss why polymer solutions behave as they do, it will be beneficial to start with an understanding of what polymers are.

### **2.1 Polymers' composition, configuration, and dimensions**

Polymers are large molecules composed of repeating monomer units. They can be the result of natural processes, and are then called biopolymers, like e.g., silk, xanthan, and guar-gum. Or they can be man-made, like the synthetic polymers, polyethylene, nylon, and polyacrylamide. Synthetic polymers are often made from monomer with a C=C bond (carbon-carbon double bond). A double bond is activated by an initiator, making it reactive (usually in form a radical) to a neighbouring monomer, creating a reactive dimer, and so on, creating polymer molecules in self-propelling chain reactions. The chain growth can stop via reaction with another active species, added quencher or quenching. Concentration of monomer, initiator and quenching techniques will determine the polymer molecules size. Due to the random nature of the reaction, the final product will be a mix of polymers with different molecular weight. The raw material for producing the monomers is usually petroleum.

Polymer molecules can be linear or branched, and if they are composed of two or more different monomer units (“monomeric segments”), they are called copolymers (as opposed to homopolymers which is only composed of one type of monomers). Copolymers composed of two different monomers units are called bipolymers, three and four are terpolymers and quaterpolymers, respectively. Copolymer can be alternating, random, blocks or grafts. Figure 4 illustrates different types of polymers. Different colours represent different monomer units. The many possible combined and vast number of different monomers that exists, have produced an almost endless amount of materials with different desirable properties, making “plastic fantastic” problematically popular.

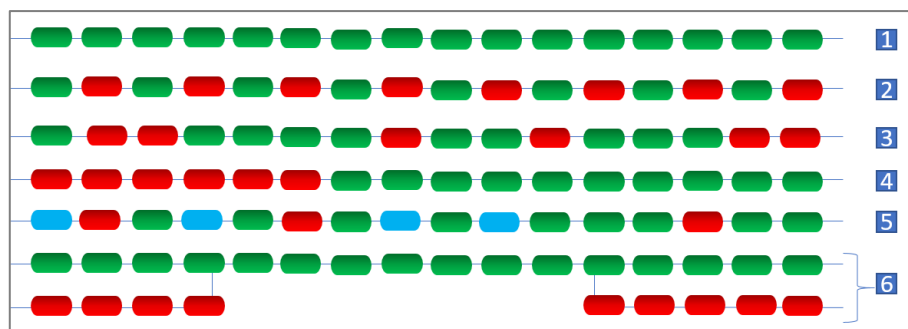


Figure 4 Illustrating different types of polymer: 1) Homopolymer 2) Alternating copolymer 3) random copolymer 4) block copolymer 5) random terpolymer 6) graft copolymer. All illustrations, except 5 and 1, are bipolymers (two different monomer units). All except 6, are linear polymers. The figure is inspired by figure on <https://en.wikipedia.org/wiki/Copolymer> (viewed 20210108), original image by en>User:V8rik.

As mentioned, polymers are large molecules. And many of their properties in solution are linked to their size. How much the viscosity increases is related to the size of the polymer molecules in solution, which is directly linked to the molecular weight of the polymer, and indirectly linked to the electrochemical interactions between the polymers, and the polymers and the solvent, that is whether the polymer shrinks because it attracts itself or expands because it repels itself.

In a solvent where the polymer neither repels nor attracts itself but floats neutrally with no interactions with it surrounding solvent or itself, the polymer molecule adopts the conformation of a random coil, a spherical “blob” (Israelachvili, 2011). The solvent where this occurs is called a theta ( $\theta$ ) solvent. The interaction between the solvent and the polymer molecule will also depend on the temperature, and the temperature where there is no electrochemical interaction between the polymer and solvent will be the theta ( $\theta$ ) temperature for that system.

But how large are the polymer molecules? Some simple calculations can be made from their molecular weight, the molecular weight of the monomers and the known length and angle of the backbone-bonds. Figure 5 illustrates how to calculate the length of each monomer, for a polymer with a carbon-based backbone where each monomer consist of two carbon atoms, as is the case for the HPAM (Hydrolyzed Polyacrylamide) based polymers studied in this work.

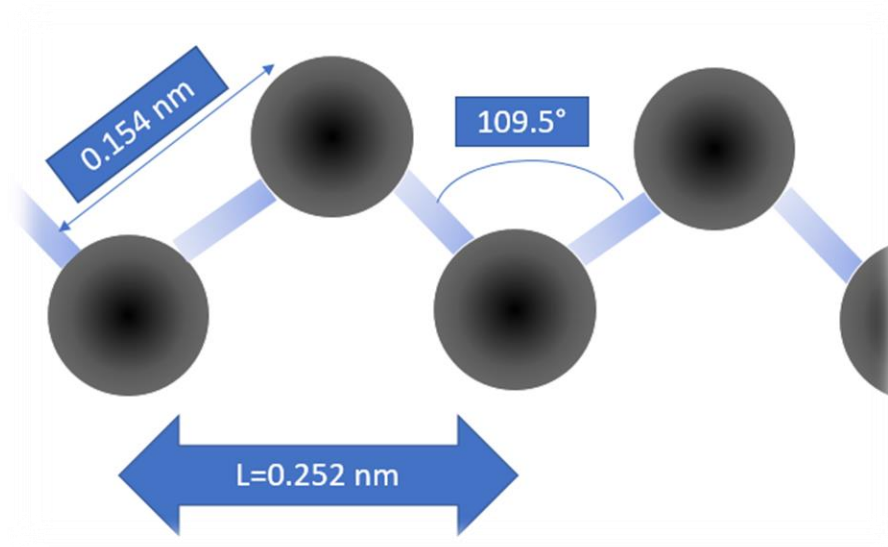


Figure 5 Illustrating how the length of a monomer unit is calculated.

From the average molecular weight of the polymer,  $M_W$  and the molecular weight of the monomers,  $M_0$ , the number of monomers,  $z$  in an average polymer molecule are

$$z = \frac{M_W}{M_0}. \quad (4)$$

As mentioned above, because of the polymerization process, a sample of polymer will have a distribution of the molecular weight, and so what we work with is the average molecular weight average by weight,  $M_W$ . The average may also be calculated as a number average,  $M_n$  but this would increase the smaller molecules influence on the molecular weight, while they compared to the larger molecules have a smaller influence on the viscosity (*Polymer Properties Database 2015-2016*).  $M_W$  and  $M_n$  can be expressed as

$$M_W = \frac{\sum_{i=1}^N N_i M_i^2}{\sum_{i=1}^N N_i M_i}, \quad (5)$$

$$M_n = \frac{\sum_{i=1}^N N_i M_i}{\sum_{i=1}^N N_i}, \quad (6)$$

where  $N$  is the total number of polymer molecules in the mix, and  $N_i$  is the number of polymer molecules with molecular weight  $M_i$ .

The contour length,  $L_c$ , of the polymers can then simply be calculated by multiplying the monomer length,  $l$  by the number of monomers,  $z$ . The contour length will be the length of the monomer when it is fully stretch without straightening the tetrahedral angle of the c-c-c-bonds.

$$L_c = zl. \quad (7)$$

At theta ( $\theta$ ) condition, without steric hindrance, the size of the random coil polymer molecules can be estimated. If we assume that the segment that can point in any arbitrary direction in relation to a neighbouring segment is the monomer, the radius of a random coil, given by a random walk is (Israelachvili, 2011):

$$R_{grw} = \frac{l\sqrt{z}}{\sqrt{6}}. \quad (8)$$

But this equation underestimates the size of the molecule coil, as it does not take into account that the molecule cannot, contradictory to a random walker, cross its own path, as it would mean that different parts of the molecule would be in the same place. For a true self avoiding random walk as defined by Amit et al. 1983 (not to be confused self-repelling and excluded volume effects), it is proposed that  $R_{gsaw}$  in 3 dimensions is proportional to  $z^{\frac{3}{5}}$  (Amit et al., 1983; Freed, 1981). In this work the following expression for the radius of the polymer coil is used:

$$R_{gsaw} = \frac{lz^{\frac{3}{5}}}{6^{\frac{3}{5}}}. \quad (9)$$

For the high molecular weight polymers used in EOR operations, with  $10^5$  monomer units, the radius of gyration from a self-avoiding random walk calculation will be  $\sim 3$  times the radius calculated from the (not self-avoiding) random walk.

Even this is probably underestimating the size, even for a non-interaction self-avoiding random walk, as the length of the segments that can adopt any direction independent of the direction of a neighbouring segment will, due to the rigidity of the bond-angle, be longer than one monomer unit (and the number of segments correspondingly smaller).

Using a molecular model build set (see Figure 6), it seems fair to say that the number of c-c- bonds in a segment should be around 4 and the length of the segments will be between 2.54 and 5.03 Å. Using the average of these two for  $l$ , and  $z$  equal to number of carbon molecules in the backbone divide by four, will probably give a better estimation of the actual size of an HPAM based polymer in a theta ( $\theta$ ) solvent. Baschnagel et al. (2004) indicates that the length of freely joint segments for polyethene should be 5 Å and be composed of 5 carbon-atoms corresponding to 2.5 monomer-units for HPAM. But since this will only impact the calculation of  $R_{gsaw}$  by increasing the result by a factor of 1.18, in this work the length of a monomer, assumed to be allowed to move independently have been used in the following calculations.

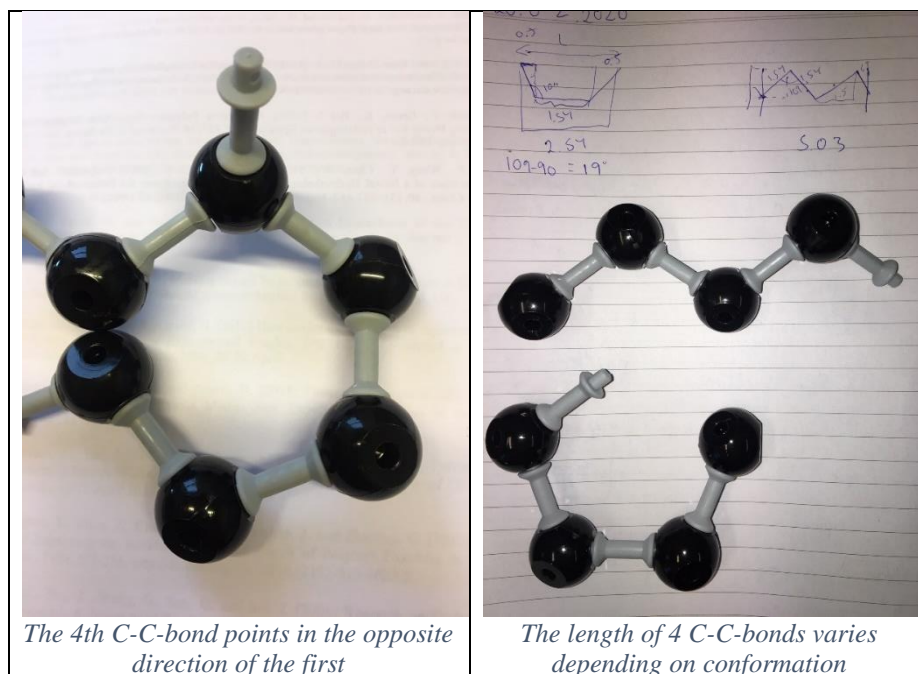


Figure 6 Molecule building set.

Israelachvili (2011) proposed, by assuming that a polymer segment occupied a volume equal to a cylinder with the same diameter as length, that the actual volume physically occupied by polymer would be equal to:

$$V_{chain} = z\pi\left(\frac{l}{2}\right)^2 l. \quad (10)$$

And the volume of the coil from the self-avoiding random walk will be:

$$V_{coil} = \frac{4}{3}\pi(R_{gsaw})^3. \quad (11)$$

Demonstrating that the fraction of the volume of the random coil physically occupied by the polymer molecule will be:

$$V_{chain}/V_{coil} \approx 4.7 \times z^{-\frac{4}{5}}. \quad (12)$$

This will mean that only a small fraction is physically occupied. For a polymer of 100 segments at theta ( $\theta$ ) conditions, approximately 10 % will be occupied. For a polymer of 100 000 segments, which is in the range of the polymers studied in this work, the number will be only 0.05% or 500 ppm.

Other quantities, such as for example adsorption, can also be estimated from the size of the polymer molecules in solution and, admittedly, some coarse assumptions.

Assuming the polymer molecules will adsorb as a mono layer of equally sized, rigid, spherical random coils, the thickness will be  $2R_{pol}$ , and the area covered by each polymer molecule will be  $\pi R_{pol}^2$ , and the area that it occupies (due to inaccessible space between the coils) is  $2\sqrt{3} R_{pol}^2$ , assuming 2-dimensional closest packing. Both the assumption that the coils are rigid, and that all the coils are equally sized is of course wrong. and will probably lead to underestimation of the amount that can be adsorbed.

From the area occupied by one polymer coil with theoretical closest 2D-packing, it is possible to calculate the adsorption capacity,  $AC$  in mass polymer per surface area for one monolayer of coils, where  $N_a$  is Avogadro's number,

$$AC = \frac{M_W}{2\sqrt{3}R_{pol}^2 N_a}. \quad (13)$$

If the specific surface area, *SSA* of the porous media is known, the mass of polymer that can be adsorbed in a monolayer can be calculated;  $AC \cdot SSA$ .

For the high molecular weight polymer with a molecular weight of 20 M Dalton and a radius of 0.14  $\mu\text{m}$ , this will give  $AC$  of  $0.5 \text{ mg/m}^2$ . For a typical specific surface area for sandstone of  $1500 \text{ cm}^2/\text{cm}^3$ , the mass of polymer that can adsorb on sandstone (under the prevailing assumptions) is  $73 \text{ g/m}^3$ , which for a sandstone of density  $2 \text{ g/cm}^3$  will give an adsorption capacity of  $0.04 \text{ mg/g}$ , which seems to be in the order expected for low polymer concentrations (Cohen & Christ, 1986; Szabo, 1975; Zhang & Seright, 2014; Zheng et al., 2000).

Interestingly, assuming a polymer coil radius from the (not self-avoiding) random walk, gives an adsorption capacity independent of the number of monomers. That is, substituting Equations (4) and (8) into Equation (13) gives  $AC$  dependent on monomer (or segment) length and molecular weight of the monomer units, but not the total number of units. Using the self-avoiding random walk gives  $AC \propto z^{-\frac{1}{5}}$ , giving a slow decrease in adsorption capacity as number of monomer units and molecular weight increases. This is not in compliance with what is generally reported in the literature. Kronberg et al. (2014) report an increase in amount adsorbed (on a neutral surface) with increasing molecular weight, explained by the stronger interaction with the surface for larger molecules. Interaction strength is not considered in the above calculations. Kim and Carty (2016) claim adsorption independent of molecular weight on clay but shows scattered results. Hirasaki and Pope (1974) propose adsorption proportional to  $M_W^{1/3}/[\eta_0]^{2/3}$ , which for  $a = 0.6$  in the Mark-Houwink equation, (Equation (23), presented later) will give results comparable  $AC \propto z^{-\frac{1}{5}}$ .

The relations above where the radius of the polymer is calculated the self-avoiding random walk will of course only be valid at theta ( $\theta$ ) conditions. The obvious advantage of this is that it is easy to calculate. Also, the above results' comparability to reported results and correlations, indicates that assuming a mono layer of adsorbed polymer, adsorbed as a random coil will give a good

first estimate of expected adsorption. This should however be confirmed by core floods at relevant conditions.

Whether polymer molecules are expanded or retracted in a specified solvent, can be estimated from viscosities of a series of equal polymers with varying molecular weight and the Mark-Houwink equation, Equation (23). This will be discussed later when intrinsic viscosity is introduced.

### ***2.1.1 Molecular structure of selected EOR polymers***

Both synthetic and naturally produced polymers (aka biopolymers) can be used and are used for Enhanced oil recovery operations. The literature review of Standnes and Skjevrak (2014) states that HPAM is the most used overall and Xanthan is the most commonly used biopolymer.

Xanthan is a high molecular weight polysaccharide with a backbone similar to cellulose with additional side chains. The side chains will form hydrogen bonds with the backbone of an adjacent xanthan polymer forming a double helix structure. A detailed description of the structure can be found in Kamal et al. (2015). So, unlike the synthetic polymers where the monomer segments are linked together only by a single C-C bond, Xanthan will in addition to the bonds between the monomers, have their conformation stabilized against deformation and strengthened against mechanical rupture by the hydrogen bonds, acting as support beams. Another consequence of the biopolymers chemical structure is their higher tolerance to salt. On the other hand, they have a lower tolerance to heat, as the helix coils out during heating. In addition, as they are almost sugar, they are tasty to bacteria and thus, prone to biodegradation.

The general chemical structures of Polyacrylamide (PAM) ( $x = 0$  and  $y = 0$ ) and HPAM ( $y = 0$  and  $x > 0$ ) are given in Figure 7. HPAM is a copolymer composed of acryl amid (IUPAC: 2-propenamid) and acrylic acid (propenoic acid) or acrylate (prop-2-enoates). It can be manufactured either by polymerization of the two monomers, or, more commonly, by hydrolysis of some of the amid groups of polyacrylamide (PAM) (Kamal et al., 2015). The polymerization process of PAM, if not adjusted not to, produces linear polymers. PAM can also be used as a viscosifying agent but is usually not used for EOR due to high adsorption in the reservoir (Kamal et al., 2015). Introducing the anionic acrylate-groups decreases adsorption on a typically

negatively charges sandstone surface, increases viscosity and decreases mechanical degradation (Kamal et al., 2015). The viscosity increases because the negatively charged groups repel each other, expanding the polymer coil in water. Unfortunately, the charged groups also render the polymer solution vulnerable to salt in the water. The ions will screen the charges, making the polymer coil shrink thus reducing the viscosity. Divalent cations may even form bridges between charged groups, causing the polymer molecules to precipitate out of solution at high concentrations of divalent ions.

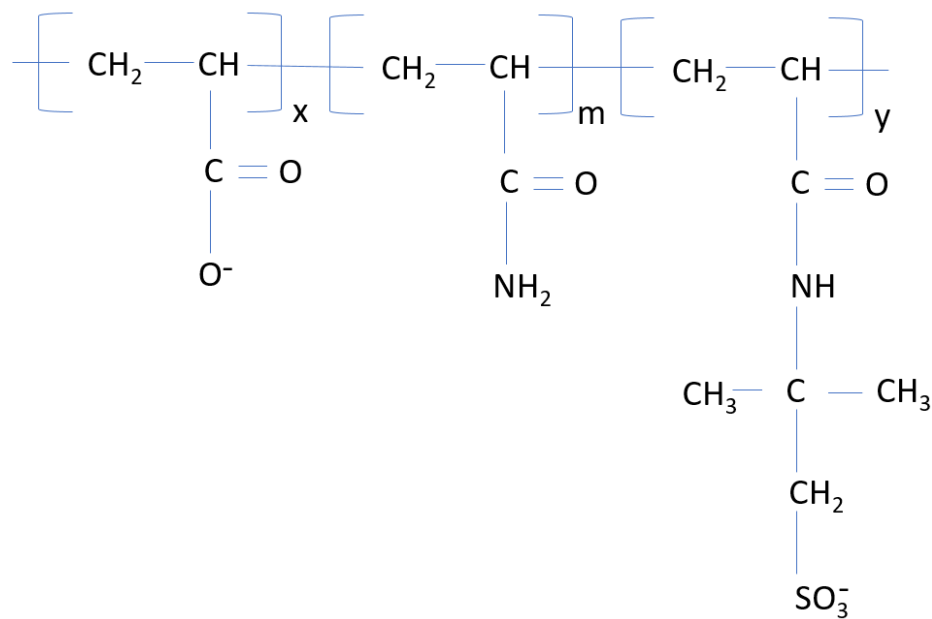


Figure 7 General chemical structure of PAM ( $x=0$   $y=0$ ), HPAM ( $y=0$ ) and ATBS-type ( $y>0$ ).

The key properties for HPAM polymer products will be the molecular weight, the molecular weight distribution, and the degree of hydrolysis. Degree of hydrolysis ( $DH$ ) is the molar ratio of the acrylic acid or acrylate monomers to the total number of monomers in the polymer, and is usually given in mol percent:

$$DH(\%) = \frac{x}{m+x+y} \cdot 100. \quad (14)$$

From the chemical structure, the molecular weight of the monomers can be calculated, from the degree of hydrolysis the average monomer molecular weight can be calculated and from the average monomer molecular weight and polymer molecular weight, the average number of monomers,  $z$  in Equations (4) through (12), can be calculated, allowing for calculation of contour length, radius of gyration and occupied volume. The HPAM polymers used in this work have molecular weight in the range of 8-20 million Dalton, which means they are composed of a couple of hundred thousand monomer units and have a contour length of 26-65  $\mu\text{m}$ .

For high salinity operations, polymer manufacturers have produced suitable candidates. Among the candidates, are the ATBS-type copolymers (see Figure 7), where the size of the sulfonated “appendix”, keeps the polymers expanded in a saline environment, retaining more of the viscosity. It also, protects the polymer from the increased tendency to mechanical and chemical degrade in saline water that HPAM experiences (Ryles, 1988; Zaitoun et al., 2012), indicating that an expanded coil, whether expanded due to electrostatic repulsion or steric hindrance, is more resistant to mechanical degradation. Kamal et al. (2015) suggest that HPAM is more resistant to mechanical degradation than PAM because PAM is more flexible, and also states that incorporation of ATBS makes HPAM stiffer, indicating that it is the increased stiffness that makes ATBS-type co-polymers more resistant to mechanical degradation.

ATBS-type copolymers are composed from acryl amid, sometimes acrylic acid (or acrylate), and Acrylamide tertiary butyl sulfonic acid (ATBS). ATBS is also frequently referred to as AMPS (2-Acrylamido-2-methylpropane sulfonic acid). The general chemical structure of ATBS-type copolymers ( $y>0$ ,) is given in Figure 7. ATBS-type copolymers can be terpolymer composed of all 3 monomer units or bipolymers ( $x=0$ ). The key property for ATBS-type polymer will, in addition to the molecular weight and degree of hydrolysis, be the fraction of ATBS-type monomers, often called degree of sulfonation ( $DS$ ) and given in mol percent:

$$DS(\%) = \frac{y}{m+x+y} \cdot 100. \quad (15)$$

As the molecular weight of the ATBS-monomers are significantly higher than the acrylamide and acrylic acid, the number of monomers, and accordingly the contour length and size calculated from random walk, will be smaller for the same polymer molecular weight for an ATBS-type copolymer compared to HPAM of the same molecular weight. The ATBS-type co-polymers used in this work have molecular weight in the range of 8-15 million Dalton, which means they are composed of around hundred thousand monomer units and have a contour length of 16-35  $\mu\text{m}$ . On the other hand, comparing HPAM and ATBS-type copolymer with the same number of monomers, the ATBS-type will be heavier, and, under some circumstances larger, due to steric hindrance, resulting in a higher viscosity. ATBS-type copolymers are more expensive than HPAM (Ruiz-Cañas et al., 2020).

Associative polymers are polymers that because of hydrophobic interactions (association) between hydrophobic segments on neighbouring polymers display increased thickening compared to polymers of the same molecular weight. The hydrophobic interactions will, under given circumstances, act as weak reversible cross-links creating a polymer solution with flow behaviour comparable to a weak gel. The hydrophobic segments can be blocks or side chains of hydrophobic oligomers or polymers (e.g., alkane chains), incorporated on to or into a water-soluble polymer (e.g., HPAM). These systems are described by Taylor and Nasr-El-Din (1998) and Dupuis et al. (2011).

In thermo-thickening associative polymers (TAPs), the associative segments of the polymer system are polymers with a lower critical solution temperature (LCST) in water. That is, polymers which at the critical temperature changes from being soluble in water to being insoluble in water, meaning it goes from a hydrophilic below LCST to a hydrophobic polymer above LCST, and the TAP, at this temperature, goes from being a purely water-soluble polymer to being an associative polymer.

The temperature at which the LCST-polymer becomes insoluble usually varies with concentration, but the temperature where it is soluble at any concentration is the lower critical solutions temperature (LCST).

For most substances, the solubility increases with increasing temperature. This is due to the favourable entropy of mixing (positive entropy): more volume is available for each of the components. For systems with LCST, the entropy of mixing is unfavourable, that is; negative. As temperature increases, the temperature times entropy increases and at some temperature, it overcomes the favourable enthalpy and there is no longer miscibility. A negative entropy of mixing is usually caused by a strong interaction between the polymer and the solvent, that prevents them from moving freely.

The concept of creating TAPs by introducing segments of polymers with LCST in water was according to Zhu et al. (2013), first described by Hourdet et al. (1994), and was further elaborated on by L'alloret et al. (1997), Durand and Hourdet (1999) and Durand and Hourdet (2000). The TAP concept is also referred to as reversible thermoassociation (L'alloret et al., 1997) and TAPs referred to as temperature-switchable polymers (Reichenbach-Klinke et al., 2018).

Of the 70 polymers reported to have LCST, conceptually all of them can be incorporated into water-soluble polymers to produce TAPs and they can be incorporated as blocks or grafts (L'alloret et al., 1997). The water-soluble polymer can be any easily copolymerized synthetic polymer (natural polymers have also been mentioned), and PAM, HPAM and copolymers with ATBS are frequently mentioned. The most frequently mentioned of the incorporated segments with LCST are polyethylene oxide (PEO) and Poly(N-isopropylacrylamide) (PNIPAM). Their chemical structure is shown in Figure 8.

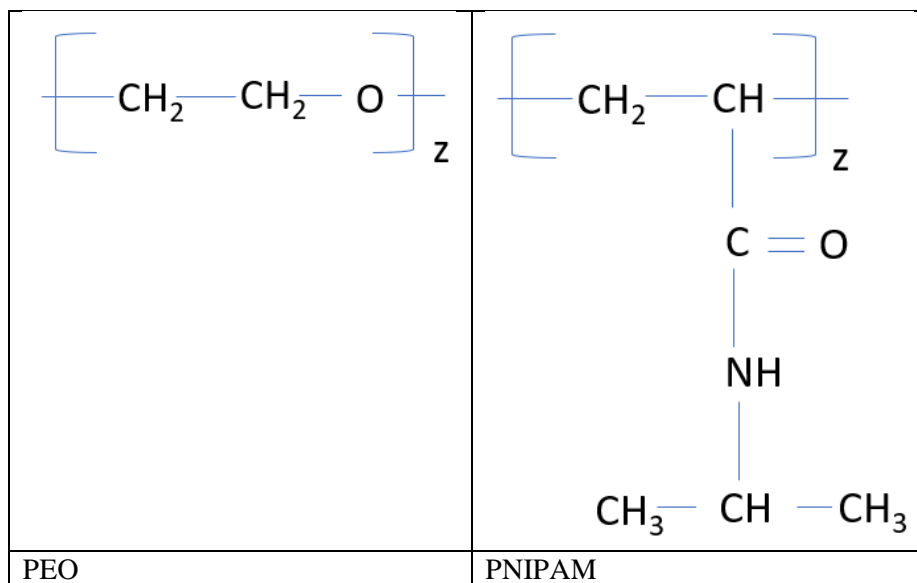


Figure 8 Molecular structure of PEO and PNIPAM.

PNIPAM's LCST, in pure water is 305K (32°C) and is virtually independent of chain length. By definition, the LCST is not dependent on concentration (as mentioned, LCST is defined as the temperature where the polymer is soluble at any concentration), but the temperature where phase separation starts will usually depend on concentration. When salt is added to the solution, the critical temperature declines. In a 1 M solution of NaCl, NaBr and NaI it drops to 293, 298 and 303K. Paradoxically, molecular dynamics simulations performed by Du et al. (2010), revealed that it is the cation that interacts directly with the PNIPAM through interaction with the oxygen of the carbonyl-group. So why is the critical temperature changed differently by the different anions? Du et al. (2010) suggest that this has to do with the strength of the cation-anion-interaction, which is weakest for the NaI. Therefore, the indirect interaction via the cation between the PNIPAM and the anion will be weakest for NaI and strongest for NaCl.

The critical temperature (LCST) of polyethylene oxide in pure water varies from 373-453K (100-180°C) depending on the molecular weight: The higher the molecular weight, the lower is the critical temperature. It is also lowered by adding salt. Presumably, the phase behaviour of PEO is linked to the hydrogen bonds favourable contribution to enthalpy, accompanied by its unfavourable

contribution to entropy, the latter becoming more dominant as the temperature increases.

Hourdet et al. (1994) synthesized 3 different polymers where only the grafting density of side chains were varied. The grafting density is the portion of monomers in the polymer backbone which has LCST-polymers grafted on to it as side chains. It was demonstrated that the behaviour of the grafted copolymer was strongly related to the thermodynamic properties of the grafts on their own, meaning that the behaviour of the copolymers as a function of temperature and grafts-characteristic can be predicted from the graft's behaviour in water prior to incorporation in the main copolymer. The backbone had a molecular weight of 500 000 Dalton (g/mol) and each side chain had a molecular weight of 5000 Dalton. The backbone was composed of acrylic acid, AA (aka hydrolyzed acrylamide) monomers, with a molecular weight of 72.1 Dalton (assuming the acid form as they do in the article). The monomer of the polyethylene side chains had a molecular weight 44.1 Dalton. The grafting density of the side chains was 0.17, 0.33 and 0.74% (from the nature of the synthesizing procedure the authors assume that the grafting is random, i.e., the side chains can be on any of the monomer units on the backbone).

From the grafting density, one can also calculate the average number of PEO side chains per polymer molecule, the average contour distance between the side chains on a polymer, and the weight percent all the PEO chains represent of the total weight of a representative polymer molecule. The average number of PEO side chains per polymer molecule will be 11.8, 22.9 and 51.3. The average distance between the side chains; 1480, 760 and 340 Å. And the amount of PEO will be 11, 19 and 34 % (w/w). All for grafting densities of 0.17, 0.33 and 0.74%, respectively. Knowing the chemical composition of the backbone and side chains, and the grafting density and using the relations in Equations (4), (7) and (9), the contour length of the backbone (1 745 nm) and side chains (41 nm) and the radius of the random coil (16 nm) is calculated at theta conditions (assuming no steric hindrance or electrochemical interference from the side chains). A to scale (~1:50 000) idealized model of the 0.17 % grafted polymer is depicted in Figure 9.



Figure 9 A simple model illustrating the dimensions of the polymer with grafting density 0.17% described by Hourdet et al. (1994). Scale  $\sim 1:50\,000$ . The purple circle has the radius of the calculated random coil of the backbone. The blue line represents the contour length of the acrylic acid backbone and the red lines represent the contour length of the PEO-side chains. The thicknesses of the lines are not to scale.

## 2.2 Bulk rheology

Water and oil are Newtonian fluids, meaning there is a linear relationship between the applied stress,  $\tau$  and the shear rate,  $\dot{\gamma}$ , and for constant temperature and pressure, the viscosity,  $\eta$  is constant, i.e., viscosity is independent of the stress.

$$\tau = \eta \dot{\gamma}. \quad (16)$$

As for most substances the oil and water viscosity will decline with temperature, and it is of course the viscosity of the oil and the water phase (injected water or polymer solution) at the reservoir temperature that will dictate the mobility ratio. Since it is the water viscosity that is changed by adding polymers, the oil viscosity will not be discussed in further detail.

Adding salt to pure water will increase its viscosity slightly, presumably because of ionic interactions and the hydrated ions carrying more momentum between laminar layers (Kwak et al., 2005). Hydrated ions are larger than the water molecules, but much smaller than the polymer molecules. The viscosity of pure water as a function of temperature can be readily found in numerous references, see e.g. CRC's Handbook of Chemistry and Physics, 63rd edition (Weast & Astle, 1983). This handbook also lists individual salts contribution to the relative viscosity. From these two, the viscosity of a salt water at a given temperature can be calculated. The viscosity of the salt waters used in this work will be listed later.

Fluids that do not abide to Newton's law of a constant ratio between applied stress and shear rate are called non-Newtonian fluids.

This can be viscoelastic fluids, thixotropic fluids, shear-thickening fluids, or shear-thinning fluids. Polymer solutions are generally shear-thinning, meaning that the viscosity declines as the shear rate (or shear stress) increases.

Polymer solutions are shear-thinning because the hydrodynamic forces of the solvent flow change the conformation of the polymer molecules in the flow field. At low shear rates (or more generally: strain rates), the rate at which the polymers have their conformation changed will be slow compared to the time it takes for them to diffuse back to their random coil conformation, hence the viscosity will be high. As the shear rate increases, the faster the polymers are stretched compared to the diffusion rate, and they will not have time to diffuse back to their relaxed state. And as their size perpendicular to the flow direction will be smaller in the stretched state, the friction between the laminar layers will decrease and the viscosity will decline.

But since the polymer chains of synthetic polymers will resist deformation and revert to their relaxed state when the influence from the flow is removed, they will display elastic characteristics when they are stretched. The polymer solutions will thus display both viscous and elastic properties. That is, they are viscoelastic fluids. The polymers' resistance to deformation when stretched in the flow field, will result in a force acting normal to the flow direction. This is the force that is manifested in the rod-climbing Weissenberg-effect (see Figure 10).

A dimensional number describing a polymer solution's viscoelastic behaviour during steady flow (motion with constant stretch history), is the Weissenberg number. According to Poole (2012), it represents the elastic forces to viscous forces, relating the rate at which the polymer is strained, strain rate,  $\kappa$  to the rate at which it can recover from strain. The rate it can recover from strain will be the inverse of the relaxation time,  $\lambda$  and  $W_i = \lambda\kappa$ . For simple shear flow,  $W_i = \lambda\dot{\gamma}$ . For low values of  $W_i$  the polymer solution will behave as a Newtonian fluid, but for  $W_i \geq 1$ , the solution will start to display non-Newtonian, anisotropic characteristics such as shear-thinning and normal forces.

Another dimensionless number, often, according to Poole (2012), confused with the Weissenberg number, is the Deborah number,  $De$  (Reiner, 1964). The

Deborah number is a dimensional number relating the relaxation time of a process to the interaction time (or observation time or measurement time),  $De = \frac{\text{relaxation time}}{\text{interaction time}}$  (Israelachvili, 2011). It compares the time it takes for a system to adjust to an action applied to it, to the duration of the action (or sometimes to how long it is observed).

During steady flow, the system has already adjusted to the action (start-up) and  $De \rightarrow 0$ , and no time-dependent properties of the system will be observed.

If the flow is not steady, the relaxation time of the system becomes important, which can be observed as a delay in reaching stable condition at the start-up, change or stop of steady flow. This is probably also what is manifested as shear-thickening (see Figure 12) in porous media. The flow will change over the length of the pore and the interaction time will be proportional to length of the pore divided by the velocity.

The Deborah number is not only of concern for viscoelastic fluids but will be important for any process with a relaxation time, that is, any process that will need some time to reach equilibrium (or relax to steady state) after being subjected to change. It will impact how energy is transferred in a process. For low or high  $De$  energy will be retained, and for  $De = 1$  maximum energy transfer, or energy dissipation will occur (Israelachvili, 2011). Imagine entering a pool of water, slowly. The water will feel soft and not be particularly disturbed, that is, little energy is transferred to the water. If the pool of water is entered faster, the water will splash, demonstrating transfer of energy. Increasing the entry rate further, will make the water feel solid and most of the energy of the impact will be absorbed by the body.

The reason why the two ( $W_i$  and  $De$ ) are often intermixed is that for certain types of flow the expression for them will coincide. According to Poole (2012), this will be the case for flow where one length scale dominates. Alternatively, according to the expressions considered above, they will coincide if the interaction time and the strain time (inverse of strain rate) are the same.

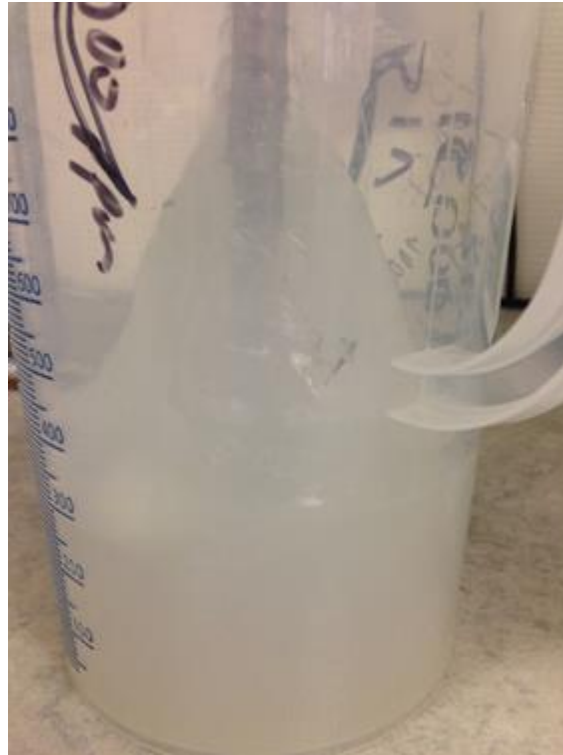


Figure 10 The rod-climbing Weissenberg-effect.

The viscosity of regular polymer solutions will, as for most fluids, decline with increasing temperature. This is mainly due to the decline in the viscosity of the solvent. For diluted polymer solutions it is often assumed that the temperature dependence follows the temperature dependence of the solvent (e.g., water). That is, the relative viscosity is assumed to be constant with temperature. As disclosed by results in e.g. Nouri and Root (1971), temperature independent relative viscosity is not a general law, but the assumption that the relative viscosity is independent of temperature has been used successfully in many works (Langaas & Stavland, 2020; Reichenbach-Klinke et al., 2013; Reichenbach-Klinke et al., 2016) and can be considered superior to measuring the viscosity of polymer solutions at elevated temperature, when reliable temperature and evaporation control can not be attained.

The relative viscosity  $\eta_r$  is generally defined as the solutions viscosity divided by the solvent's viscosity,

$$\eta_r = \frac{\eta_p}{\eta_w}. \quad (17)$$

As the concept dictates and name reveals, the viscosity of TAPs increases with increasing temperature, or more precisely, it increases significantly at a specific temperature. At the low temperatures where the incorporated active moieties are water-soluble, the polymers behaviour will closely resemble that of the main polymer (e.g., HPAM), whereas at high temperature, above a certain concentration, it will behave as an hydrophobically associating polymer with a very shear-thinning flow behaviour similar to a weak gel.

At very low shear rates, associating polymers have also been reported to be shear-thickening. This has been attributed to the need for sufficient deformation of the polymers to favour intermolecular association over intramolecular association (Bokias et al., 2000; Zhong et al., 2009). In other words, at very low shear rates, the polymers are coiled up and the associative groups interacts with associative groups in the same polymer. As the shear rate increases, the polymer is deformed and some of these interactions are broken, exposing the associative groups to interact with exposed groups on neighbouring polymers, leading to a higher viscosity. This is also why associative polymers have to be above a certain concentration for associative viscosity increase to occur. As shear rate is increased further, the intermolecular association is broken more often compared to have fast it is formed, and one has entered the shear-thinning regime.

So, polymer solutions have a more complicated relationship between the shear stress and shear rate than the constant viscosity term in equation (16). Both regular polymer and TAPs display shear-thinning behaviour. Shear-thinning can be described by a power law relationship between shear rate and viscosity, or more commonly for the diluted polymer solutions for enhanced oil recovery, by the Carreau model or an improved version of the latter: the Carreau-Yasuda model, capable of capturing more details.

For a power law fluid, the shear dependent viscosity is described by

$$\eta = K(\dot{\gamma})^{n-1}. \quad (18)$$

Here,  $K$  is the flow consistency index and  $n$  is the flow behaviour index. The power law model fails to capture the Newtonian behaviour (constant viscosity) displayed by EOR polymer solutions at low shear rates and underestimates the

viscosity at high shear rates. These are both better captured by the Carreau model and the Carreau-Yasuda model, which can describe the change from Newtonian to shear-thinning behaviour at a critical shear rate.

$$\eta = \eta_{\infty} + (\eta_0 - \eta_{\infty})[1 + (\lambda \dot{\gamma})^y]^{\frac{n-1}{y}}. \quad (19)$$

Equation (19) show the Carreau-Yasuda model, which for  $y = 2$  is the Carreau model.  $\eta_{\infty}$  is the viscosity at infinite shear rate, typically equal to the solvent viscosity,  $\eta_0$  is the viscosity at the Newtonian plateau, also known as Newtonian viscosity or the zero-shear rate viscosity,  $\lambda$  is the invers of the critical shear rate at which the polymer behaviour changes from Newtonian to shear-thinning, that is, it is the timescale at which the hydrodynamic forces overcome the random Brownian motion.  $\lambda$  has the dimension of time and is the relaxation time of the polymer solution.

Examples of the 3 models are shown in Figure 11. For comparison, measured values of the viscosity as a function of shear rate for 1000 ppm of a high molecular weight HPAM in low salinity NaCl water (0.5%) is also included. The viscosity was measured at 20°C by a cone and plate geometry by an Anton Paar MCR301 Rheometer. This is the same polymer solution as one of the solutions studied in Åsen et al. (2019). In the power law model, the flow consistency index,  $K = 55 \text{ cPs}^{n-1}$  and  $n = 0.64$ . For the Carreau-Yasuda model,  $\eta_{\infty} = 10 \text{ cP}$ ,  $\eta_0 = 80 \text{ cP}$ ,  $\lambda = 1.2 \text{ s}$ ,  $y = 1.1$  and  $n = 0.3$ . For the Carreau model, the same values as for Carreau-Yasuda are used except for  $y \stackrel{\text{def}}{=} 2.0$  and  $n = 0.15$ .

The figure clearly demonstrates the power law models weaknesses at low and high shear rates. It also reveals that the Carreau-Yasuda-model is better at capturing a smooth transition from Newtonian to shear-thinning behaviour (caused by molecular weight distribution) compared to the Carreau model. That be said, most of the polymer solutions studied in this work have a lower bulk viscosity than this solution, and their behaviour is sufficiently captured by the Carreau model which is used in the majority of the work described in this thesis. For high polymer concentrations, and high viscosity it might be more relevant to use the power law model, as for concentrated solution it is very seldom to observed Newtonian plateaus at practical shear-rates.

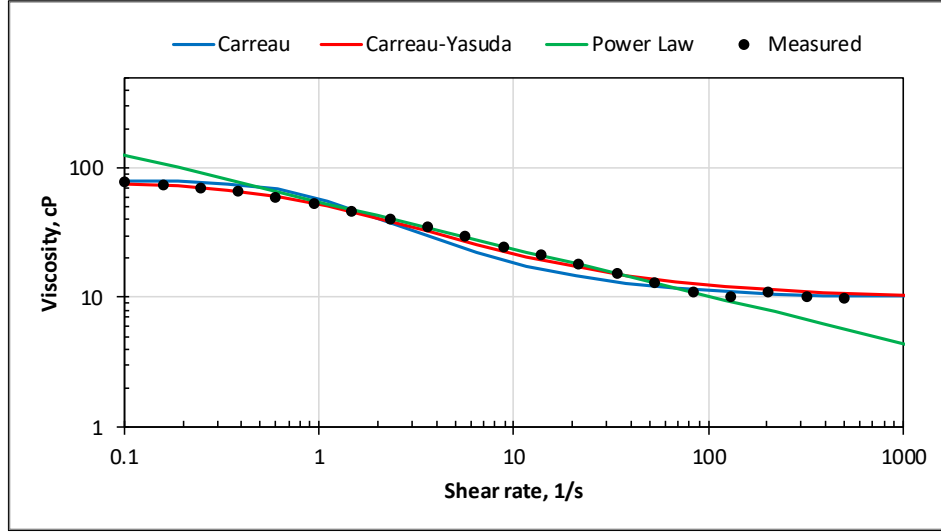


Figure 11 Shear-thinning models and measured viscosity.

An important property for a polymer/solvent system is the intrinsic viscosity. The intrinsic viscosity gives a measure of the individual polymer molecules' contribution to the viscosity. As the concentration approaches zero, the contribution of polymer-polymer interaction on the viscosity is eliminated. Thereby, the size of the polymer molecules will be the only contributor to the increase in viscosity of the solvent, and from the intrinsic viscosity the size and molecular weight of the polymer molecules in said solvent can be calculated from the Mark–Houwink equation, which is introduced later, see Equation (23).

Intrinsic viscosity,  $[\eta_0]$  is defined as:

$$[\eta_0] = \lim_{c \rightarrow 0} \frac{\eta_0 - \eta_s}{\eta_s c}. \quad (20)$$

Here,  $c$  is the concentration,  $\eta_s$  is the solvent viscosity, and  $\eta_0$  is the zero shear-rate viscosity of the polymer solution.

The intrinsic viscosities can be estimated from Taylor expansion, see Equation (22) of the Martin equation (21). Note that the expansion is only valid for low values of  $[\eta_0]c$ , that is when the viscosity is measured at relatively low concentrations. If  $[\eta_0]c > 1$ , the Taylor Expansion is not valid.

$$\eta_0 = \eta_s (1 + [\eta_0]c e^{k'[\eta_0]c}), \quad (21)$$

$$\eta_0 = \eta_s \left( 1 + [\eta_0]c + k'[\eta_0]^2 c^2 + \frac{k'^2}{2} [\eta_0]^3 c^3 + O(c^4) \right). \quad (22)$$

In practice, calculating the intrinsic can be done by solving Equation (22) with respect to  $x = [\eta_0]c$ . The relative viscosity,  $\eta_0/\eta_s$  is known from measurements and  $k'$  is set equal to 0.5. First, the third and fourth order terms are omitted and a first approximation of  $x$  is calculated by solving the second order equation. Then the first approximation is used as the initial guess, and omitting the fourth term,  $x$  is calculated by Newton's method.

An alternative approach to determine the intrinsic viscosity, is to measure the viscosity,  $\eta_0$  at decreasing concentrations, plot the reduced viscosity,  $\frac{\eta_0 - \eta_s}{\eta_s c}$  as a function of concentration, and extrapolate to zero concentration.

A relation between the molecular weight,  $M_V$  and the intrinsic viscosity,  $[\eta]$  is given by the Mark–Houwink equation.  $M_V$  is the “viscosity averaged molecular weight”, and  $M_n < M_V < M_W$ , that is,  $M_V$  is in magnitude, in-between the number averaged and the weight averaged molecular weight (*Polymer Properties Database 2015-2016*).

$$[\eta_0] = KM_V^a = A'R_g^{a'} \quad (23)$$

Here,  $K$  and  $a$  are polymer/solvent dependent constants, and the value of  $a$  indicate whether the solvent is good, a theta ( $\theta$ ) solvent or a poor solvent for said polymer;  $a > 0.5$  indicate a good solvent (expanded polymer),  $a = 0.5$  indicate a theta ( $\theta$ ) solvent (no interaction solvent/polymer) and  $a < 0.5$  indicate a poor solvent (polymer coil shrinks). Hence, for intrinsic viscosity data for a series with different molecular weight of the same polymer type,  $a$  can be calculated for said polymer type, and one can determine whether the solvent in which the intrinsic viscosities are calculated is good, theta or poor.

Intrinsic viscosity data for series of polymers with different molecular weight and same degree of hydrolyzes from Stavland et al. (2010) indicate that HPAM with a degree of hydrolyzes of 20 and 30% will be expanded in synthetic sea

water (SSW). That is, the exponent in Mark-Houwink equation will be above 0.5 and SSW can be considered a good solvent for these polymers. An HPAM with 10% hydrolyzes will be around  $\theta$ -condition, possibly with a tendency to be a slightly contracted. This is assuming that the listed molecular weight,  $M_W$  has the same proportionality to  $M_V$  for the range of molecular weight within a series.

### 2.2.1 Laminar flow in circular tubes

By measuring the differential pressure across circular tubes, the viscosity of the fluid flowing in the tube can be calculated. For laminar flow of a Newtonian fluid in a tube with internal diameter (ID) of  $2R$  and length of  $l$ , the differential pressure,  $\Delta P$ , at volumetric injection rate,  $Q$  is given by the Hagen-Poiseuille equation. Assuming that this also holds for polymer solutions, the differential pressure across the capillary with polymer,  $\Delta P_p$  and with water,  $\Delta P_w$  can be used to calculate the viscosity,  $\eta_p$  of the polymer solution as long as the water viscosity,  $\eta_w$  is known. The validity of this is demonstrated in Åsen et al. (2021) (Paper 3).

$$\Delta P = \frac{8Q\eta l}{\pi R^4} \Rightarrow \frac{\Delta P_p(T,Q)}{\Delta P_w(T,Q)} = \frac{\eta_p}{\eta_w} \stackrel{\text{def}}{=} \eta_r. \quad (24)$$

The shear rate at the walls in capillary tubes,  $\dot{\gamma}_{ct}$  can also be derived from the Hagen-Poiseuille equation. The shear stress,  $\tau = \frac{F}{A} = \frac{\Delta P \pi r^2}{l 2\pi r}$ , and by combining this relation with Equation (24) and Equation (14) we get the following expression for the shear rate at the wall of a circular tube with radius  $R$ .

$$\dot{\gamma}_{ct} = \frac{4Q}{\pi R^3} = \frac{4\langle v \rangle}{R}. \quad (25)$$

Strictly speaking, since derived from the Hagen-Poiseuille equation, this will only hold for Newtonian fluids. For power law fluids, Sorbie (1991) proposed a correction factor of  $\frac{1+3n}{4n}$ , which for  $n = 0.64$  will give a correction factor of 1.14. To that end, in this work, Equation (25) is used to calculate shear rate in capillary tubes for both Newtonian and non-Newtonian fluids.

### 2.2.2 Turbulent flow in large pipes

The Hagen-Poiseuille equation is only valid at laminar flow. If the volumetric injection rate is increased, so that inertial forces dominant over viscous forces, the flow can become turbulent, and the pressure drop increases (above what is predicted by Hagen-Poiseuille equation). The balance between inertial and viscous forces is defined by the Reynolds number,  $Re$ . In circular tubes for a fluid with density,  $\rho$  the Reynolds number is,

$$Re = \frac{2Q\rho}{\eta R\pi}. \quad (26)$$

For  $Re < 2300$  the flow is laminar, for  $Re > 4000$  the flow is turbulent.

From the Darcy-Weisbach equation (which gives the pressure drop across cylindrical pipes) and Equation (16), the shear rate at the wall at both laminar and turbulent flow can be expressed as:

$$\dot{\gamma}_w = \frac{f\rho Q^2}{8\eta\pi^2 R^4}. \quad (27)$$

Here  $f$ , is the friction factor which for laminar flow is inversely proportional to the Reynold number,  $f = 64/Re$  which leads us back to Equation (25); a shear rate that is independent of viscosity (and density). Note: The laminar friction factor is deduced from Poiseuille. For turbulent flow, many forms of the friction factor have been proposed usually in some form where it is no longer directly inversely proportional to the Reynolds number, but rather;  $f = a/Re^\beta$ , where  $\beta < 1$  (and not necessarily constant). Consequently, the shear rate is no longer independent of the viscosity. This further complicates calculations for flow of polymer solutions as the viscosity is also a function of shear rate. In addition, the drag reduction ability of polymer solution at turbulent flow must also be taken into account, meaning that the friction factor will decrease if polymer is added. That be said, from two assumptions we can get a relatively neat expression for the turbulent shear rate. Assuming  $\beta = const$ ,  $a_p$  can easily be calculated from the polymer solutions drag reduction, DR,

$$DR \stackrel{\text{def}}{=} \frac{f-f_p}{f} \rightarrow a_p = a(1 - DR). \quad (28)$$

And assuming that the shear rate is so high that the viscosity approaches a fixed value,  $\eta_\infty$ , we get:

$$\dot{\gamma}_{tw} = \frac{a_p \rho^{1-\beta} Q^{2-\beta}}{2^{3+\beta} \eta_\infty^{1-\beta} \pi^{2-\beta} R^{4-\beta}}. \quad (29)$$

## 2.3 Porous media behaviour of polymer solutions

### 2.3.1 Mobility reduction

For a porous media with constant cross section area (i.e., a cylindrical porous media core) of length,  $L$ , permeability,  $k$  and cross section area of  $A$ , the differential pressure across the core,  $\Delta P$  is given by Darcy's law:

$$\Delta P = \frac{\eta L Q}{k A}. \quad (30)$$

From (30) we then get

$$\frac{\Delta P_p}{\Delta P_w} = \frac{\eta_p / k_p}{\eta_w / k_w} = \frac{\lambda_w}{\lambda_p}. \quad (31)$$

Hence, a both pertinent and straightforward method for measuring the effectiveness of a polymer solutions ability to alter the mobility ratio between the injected phase and the oil phase, see Equation (2), is to measure the differential pressure across linear cores, first with water, and compare the pressure drop to the pressure drop attained by the subsequent injection of polymer solution at the same volumetric flow rate,  $Q$ . We then get the resistance factor for linear cores,  $RF$ , also commonly referred to as mobility reduction.

$$RF = \frac{\Delta P_p}{\Delta P_w}. \quad (32)$$

Measuring the differential pressure captures the effect of both viscosity increase and permeability alterations, and the mobility ratio improvement by injecting polymer is  $\propto RF^{-1}$ .

$$\frac{\Psi_{p/o}}{\Psi_{w/o}} = \frac{1}{RF}. \quad (33)$$

By injecting water after polymer injection and measure differential pressure when steady state is attained, the residual resistance factor,  $RRF$  is given by

$$RRF = \frac{\Delta P_{w,post}}{\Delta P_{w,pre}}. \quad (34)$$

It is generally believed that the residual resistance factor captures the permeability alteration during the polymer flood (Nødland, 2019), so that:

$$RF = \frac{\eta_p}{\eta_w} \times RRF = \eta_r \times RRF. \quad (35)$$

The permeability reduction,  $RRF$  is a result of the adsorbed layers (at least if it is measured by injecting water in the opposite direction, freeing mechanically trapped polymer molecules). By modelling the porous media as capillary tubes with pore radius,  $R_{pm}$  with a mono layer of adsorbed polymers and using the Hagen-Poiseuille equation, see Equation (24), we get the following expression for  $RRF$ .

$$RRF \stackrel{\text{def}}{=} \frac{\Delta P_{w,post}}{\Delta P_{w,pre}} = \left(1 - \frac{2R_{pol}}{R_{pm}}\right)^{-4}. \quad (36)$$

For a high molecular weight polymer with a radius of  $0.14 \mu\text{m}$ , which is the estimated  $R_{gsaw}$ , radius of gyration at theta ( $\theta$ ) conditions for the high molecular weight HPAM studied in this work, calculated from Equation (9) in chapter 2.1, this will give a permeability reduction of 1.12 in a sandstone with pore throat radius of  $10 \mu\text{m}$ . Despite all the assumptions, the stipulated  $RRF$  is in the ballpark of what is generally observed, after injecting substantial amounts of water, again supporting the usefulness of assuming adsorption of a monolayer of random coils.

In a post polymer water-flood in a core, it is not uncommon to have to injects  $10^2$  pore volumes (PV) of water to reach stable end-point permeability, i.e. residual resistance factor. Such volumes are not realistic at field scale, and a

higher permeability reduction will be sustained in the post-polymer water-flood, which will have positive influence on the sweep.

This may also be an appropriate place to mention, that RRF is not only direction dependent, but will also be rate dependent, as adsorbed polymers also align themselves in the flow field, and can over time also change their conformation to a flat or brush structure (Israelachvili, 2011).

### **2.3.2 Porous media rheology**

Since the polymer solutions flow behaviour in a reservoir will also be shear dependent, having an expression for the shear rate in a porous media will be useful. There is no single shear rate in a porous media, as the shear rate varies from point to point, and an average value must be used. The common practice is to calculate the average shear rate,  $\dot{\gamma}_{pm}$  in the porous media by assuming the porous media to be a bundle of (equal size) capillary tubes. The radii of the tubes are related to permeability and porosity as  $R = \sqrt{\frac{8k}{\varphi}}$ , where  $\varphi$  is the porosity. The shear rate can then be found from Equation (25):

$$\dot{\gamma}_{pm} = \frac{4\alpha v}{\sqrt{8k/\varphi}} = \frac{4\alpha Q}{\pi R^2 \sqrt{8k\varphi}} \quad (37)$$

$\alpha$  is a correction factor to correct for the simple bundle of tubes picture of a porous medium. This approach is analogue to Chauveteau and Sorbie (1991), Cannella et al. (1988) and Teeuw and Hesselink (1980). In this work  $\alpha = 2.5$ , is used, as proposed for sand packs by Chauveteau and Sorbie (1991).

The shear-thinning behaviour of polymer solutions observed in steady shear laminar flow, is explained by the polymer molecules tendency to align themselves in the flow field, decreasing the internal friction between the laminar layers flowing at different velocities. During porous media flow, the flow field will be constantly changing as the solution is accelerated through narrow pores, meets interconnecting flow stream and changes direction. The polymer will experience both shear flow (velocity gradient perpendicular to the flow direction) and elongational flow (velocity gradient parallel to the flow direction).

At low velocities, that is low porous media shear rates, the behaviour will still have a Newtonian plateau, followed by shear-thinning, where  $RF$  will decline with increasing  $\dot{\gamma}_{pm}$ . At typical in-depth reservoir propagation rates, corresponding to a shear rate of  $6 \text{ s}^{-1}$ , the polymer solution in Figure 11 will be in the shear-thinning regime. As discussed above since  $k_p < k_w$ , it is reasonable to assume that  $RF(\dot{\gamma}_{pm})$  will be slightly higher than the relative viscosity,  $\eta_r$  at  $\dot{\gamma} = \dot{\gamma}_{pm}$ . On the other hand, if one accounts for the polymer solutions permeability reduction, as measured by  $RRF$ , see equation (35), resulting values for the relative viscosity in the porous media,  $\eta_{r,pm} = \frac{RF}{RRF}$ , lower than bulk relative viscosities have been reported at low shear rates (Zaitoun & Kohler, 1987). This slip-effect is attributed to concentration gradient in the flow field (perpendicular to the flow direction), giving a lower concentration of polymer molecules close to the wall (depleted layer at the wall due to steric hindrance or, possibly, wall depletion caused by lower flux at the wall) (Nødland, 2019).

As  $\dot{\gamma}_{pm}$  increases further, synthetic polymers will experience shear-thickening. The polymer molecules will not have time to change their conformation to the flow field, and the shear-thickening behaviour of synthetic polymers in porous media becomes evident (Figure 12). If  $\dot{\gamma}_{pm}$  is further increased, synthetic polymers will experience mechanical degradation. A decline in  $RF$  will be observed, accompanied by a decline in effluent viscosity. This is because the forces on the polymer molecules have been so harsh that the backbone of the polymer molecules ruptures, decreasing the molecular weight of the polymer molecules, so that the viscosity is permanently and irreversibly reduced. Figure 12 shows the relative bulk viscosity of the injected solution as a function of rheometer shear rate, mobility reduction in a 3 cm Bentheimer core as a function of porous media shear rate, and the normalized remaining viscosity, see Equation (39), as a function of the shear rate where the effluent sample was degraded for the 1000 ppm high molecular weight HPAM in 0.5% NaCl studied in Åsen et al. (2019) (Paper1).

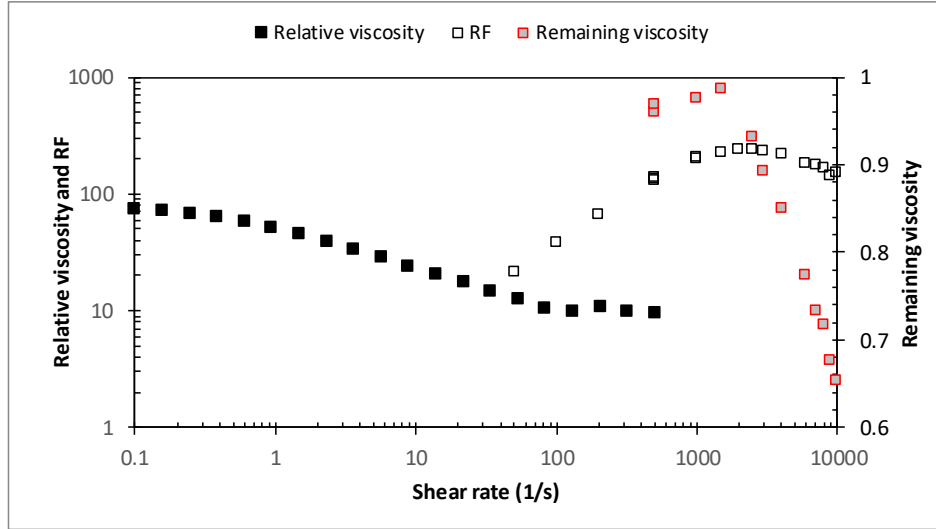


Figure 12 The relative viscosity (closed black symbols) is the shear-thinning viscosity of the fresh polymer solution plotted against the shear rate in the rheometer. RF (open black symbols) is the mobility reduction in the porous media as a function of the porous media shear rate. The remaining viscosity (normalized) of the effluent (red open symbols) is plotted against the porous media shear rate at which the polymer solution was degraded. The polymer solution is 1000 ppm high molecular weight HPAM in 0.5%NaCl.

Shear-thickening and mechanical degradation of synthetic polymers in porous media have been extensively studied and several scaling laws have been proposed (Maerker, 1975; Seright, 1983; Stavland et al., 2010). It is often shown that mechanical degradation scales with the shear rate (Culter et al., 1975; Stavland et al., 2010; Stavland et al., 2021). To add to the possible misconception that it is the shear forces that degrades the polymer, mechanical degradation is also often referred to as shear degradation. But as mechanical degradation does not increase with increasing length of a tube (Jouenne et al., 2018; Stavland et al., 2021), which corresponds to increasing time exposed to the same shear rate, but increases with the number of passes in a capillary tube (Culter et al., 1975; Jouenne et al., 2018), it seems reasonable to assume that mechanical degradation is caused by the elongational flow at the inlet of the flow constriction. And that the reason why mechanical degradation scales with the shear rate, is that the shear rate is proportional to the stretch rate,  $\dot{\epsilon} \propto \dot{\gamma} \tan(\theta)$ , where  $\theta$  is the incline angle of the constriction and  $\dot{\epsilon} = \delta v / \delta x$ . In a porous media, the inlet of the flow constriction will be the entrance of the pore throats.

The porous media rheological behaviour of shear-thickening and mechanical degradation is typical for synthetic polymers. Most biopolymers will not display this behaviour in porous media, at relevant velocities. They behave, due to the reinforced chemical structure described above for Xanthan, as rigid rods. They align themselves in the flow field, displaying strong shear-thinning behaviour, both in steady shear flow and porous media flow, but will not have their conformation changed. But at very high porous media rates, even they will not have time to react to the rapid changes in the flow, resulting in shear-thickening and even degradation (Jolma et al., 2017)

To understand the rheology of polymer solutions in a porous media, some simple calculations relating polymer dimensions to porous media dimension might be useful. A sandstone oil reservoir will be a porous media made from deposited sand with interconnected pore spaces where hydrocarbons can be stored and flow. Irregular sand grains in random packing results in a disordered network of larger pore bodies and narrower pore throats.

According to Carman-Kozeny (Carman, 1956; Kozeny, 1927) the following relation can be found between particle size  $D_p$ , porosity,  $\varphi$  tortuosity,  $\tau$  and permeability,  $k$ :

$$k = \frac{D_p^2 \varphi^3}{72\tau(1-\varphi)^2}. \quad (38)$$

In our work we have used Bentheimer, Berea and unconsolidated sand as model rocks for generic oil reservoirs suitable for polymer flooding. Here the approximate dimensions of Bentheimer and very idealized pore geometry will be used to show some simple dimension relations. In the equation for calculating shear rate in porous media, Equation (37), the radius of the pores is assumed to be given by:  $R^2 = \frac{8k}{\varphi}$ . For a Bentheimer rock with a typical porosity of 0.2 and permeability of 2 Darcy, this will give a pore radius of 9  $\mu\text{m}$ , or for the love of round numbers 10  $\mu\text{m}$ . Since the narrow pore throats will give the largest contribution to the permeability, this is set as the value for an imagined model pore throat. Values for pore throats and pore bodies of Bentheimer have been proposed to be 6-15  $\mu\text{m}$  and 7-30  $\mu\text{m}$ , respectively. Values reported in the

literature vary and will depend on throat-body-definition and measuring techniques, see e.g. Maloney et al. (1990) and Kruschwitz et al. (2017).

Here, a model pore body with twice the radius of the pore throat is used. The model pore space with a cylindrical pore body with  $l = d = 40 \mu\text{m}$ , connected to, for connectivity, two cylindrical pore throats with  $l = d = 20 \mu\text{m}$  is depicted in Figure 13. If we then imagine that random coil of the High molecular weight HPAM referred above with radius of  $0.14 \mu\text{m}$ , to be the size of a ping-pong ball (radius  $\sim 1.4 \text{ cm}$ ), the volume of the pore body will be the size of two of my offices (that is: the size of my managers office) and the cross-section area of the pore throats will be the  $\sim$ size (area) of a double door. Figure 13 shows the model pore, the size of the random coil and the contour length of the polymer molecule to scale. It is thus easy to accept that it is not forcing the individual polymer coil through the pore throats that causes mechanical degradation. The polymer coil will also be much more flexible than a ping-pong ball. It is, as discussed above, mostly solvent, and holds its form by nothing more than a series of coincidences; there are many more ways for it to be a random coil than in a stretched state. But in its fully stretched state (stretched without bending the C-C-C-angles), upscaling the contour length of  $65 \mu\text{m}$  and width of  $2.5 \text{ \AA}$  (width suggested by Israelachvili (2011)) by factor  $1\text{E}+05$ , the ping-pong-ball-sized polymer coil will be  $6.5 \text{ m}$  longer and only  $\frac{1}{4}$  of a millimetre thick (or 3 hairs' breadth).

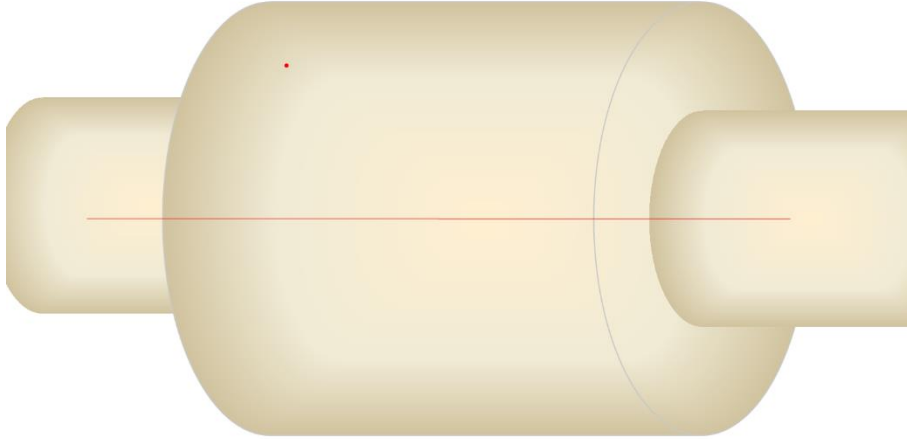


Figure 13 The random coil (red dot), its contour length (red line) and model pore body and pore throat to scale. The width of the line is **not** to scale, and that conformation (fully stretched) not realistic (very improbable).

For a concentration of 1000 ppm, there will be 1.5 million coils (equivalent to the number of hairs on 10-15 people's heads) floating around in the volume of the pore body, with the coil volume occupying 35%. From this it is easy to imagine that the polymer molecules will on occasions become entangled, they will during flow be stretched, and as they enter the narrower pore throats and the fluid stream is accelerated, different parts of the long polymer or polymer tangles will experience different velocities and acceleration. For slow flow the polymer molecules will have time to reptate out of the tangles, but for fast flow the tangles will tighten, making them more resistant to flow (shear-thickening) and if the tangle is tightened further it can be bent to snap (mechanical degradation). It is like pulling a brush through very long hair. If the brush is pulled slowly through the hair, the hair strands are being pulled apart and becomes untangled. If it is pulled too fast it creates more tangles than are being untangle, the brush gets stuck, and if more force is used to pull the brush, something must give. The tangle analogy may be said to contradict the result in Stavland et al. (2021) (Paper 2), as there it is demonstrated that higher concentration protects against mechanical degradation, and concentrated solutions should have more entanglement. But this can be explained by the force being distributed to more polymer molecules. Continuing with the brush and hair analogy, it is much easier to pull the hair of the scull if you brush a

tight tangle with only a few hairs, as compared to if you are pulling the brush through a full brush of hairs. For hair, the root is the weakest point and is what gives. If hair itself is being pulled to break, where it breaks seems to be rather random. If a knot is being tied on it, it breaks at the knot (with perhaps a tendency to break easier than without the knot).

Jouenne et al. (2018) and Zaitoun et al. (2012) suggest that mechanical degradation occurs as random scission (cleaving), at least in the semi diluted regime. Mechanical degradation is also more pronounced the higher the molecular weight (Martin, 1986) and will target the high-molecular weight fraction of a polymer solution. This is presumably because the chance of different parts of the polymer being pulled in different directions or bent to break are larger and the “grip” is harder (as it applied to a longer part) when the polymer is larger. This consideration would indicate that although the breakage can occur anywhere on the chain, the probability will increase towards the centre, which is reported by Kim et al. (2000) for low concentrations. Even though the C-C bond is considered strong (~100 kcal/mol), only one of them (~0.5 attojoule), if near the centre of the polymer, must break to halve the molecular weight of that polymer. And the force (e.g., viscous friction force) needed to break it can be distributed over the length, in opposite directions (direction of the polymer) on each side of the breaking point. The smaller molecules resulting from the break, will then be released from the forces and the chance of them breaking will be smaller both because they will have a smaller tendency to entangle, it will be easier for them to reptate out of a tangle, and the forces exerted on them by the same friction will be smaller.

If one accepts the above considerations, it seems reasonable that for each distortion in the flow field only some of the polymer molecules will be under conditions entailing degradation. The polymers surviving the distortion, may then suffer degradation during subsequent distortion (passing of the next pore throat or constriction).

As shown by Mark-Houwink equation, reducing the molecular weight by a factor of  $x$  will reduce the intrinsic viscosity, by a factor of  $(1/x)^a$ . That is, for a degraded solution where the molecular weight has been reduced to one third of the original molecular weight, and Mark-Houwink exponent,  $a$  is 0.5 (theta ( $\theta$ ) conditions), the intrinsic viscosity is reduced to 58% of the original.

As it is much easier to measure the viscosity of a polymer solution, than the molecular weight, degradation is usually monitored by decline in viscosity, and reported as normalized remaining viscosity,  $\eta_N$  or normalized degradation:  $\eta_D = 1 - \eta_N$ .

$$\eta_N = \frac{\eta_0 - \eta_s}{\eta_{0i} - \eta_s}. \quad (39)$$

Here,  $\eta_0$  is the zero-shear rate viscosity of the degraded polymer,  $\eta_{0i}$  is the initial zero-shear rate viscosity (before injection) and  $\eta_s$  is the viscosity of the solvent (water in our case). The expression for  $\eta_N$  is equal to the ratio of the intrinsic viscosity of the degraded solution (effluent) to the intrinsic viscosity of the undegraded (fresh solution).

Regarding the statement to use the zero-shear rate viscosity to monitor degradation: This is important for two reasons. 1) It is only in this regime  $\eta_N$  is equal to the ratio of the intrinsic viscosities. And 2) in the shear-thinning regime, the attained value for  $\eta_N$  will depend on the shear rate. At high shear rate the viscosities,  $\eta$  and  $\eta_i$  will approach each other, and the calculated degradation will seem smaller. That be said, it is not always possible to attain the zero-shear rate viscosities, particular if the Newtonian plateau only exists at very low shear rates where it's difficult to get good readings, or if an in-line viscometer it used, which only gives viscosity at the prevailing shear rates given by the injection rates. In those cases, it is important to use  $\eta$  and  $\eta_i$  measured at the same shear rate and clearly state what shear rate that is.

Degradation can also be monitored by declining  $RF$  from core segment to core segment as is demonstrated in Åsen et al. (2019) (Paper 1).

Thermo-thickening associative polymers (TAPs) as discussed above have several properties which should be beneficial for enhanced oil recovery. They are soluble in water at top-side conditions. They are not negatively influence by salt, if anything, their favourable trades are enhanced by salinity. Their resistance to flow is highest deep in the reservoir, at low rates and high temperature, and low in the high rate, often lower temperature of the injection area. Since their thickening ability does not merely rely on the molecular weight of the polymer molecules, lower molecular weight polymers can be used than for a traditional polymer flood, meaning that the polymers are less susceptible

to mechanical degradation and injectivity is improved. From the literature (Durand & Hourdet, 2000; L'allouet et al., 1997; Lara-Ceniceros et al., 2014; Zhu et al., 2013), it seems clear that their properties can be tailored to the specific condition of a candidate reservoir, by changing the size, grafting density and chemical structure of the side chains and molecular weight and chemical structure of the backbone. For example, the side chains or blocks can be copolymerized with hydrophobic or hydrophilic monomers to decrease or increase the association temperature. Thermo-thickening associative polymers' resistance to flow is also enhanced by the mere presence of the porous media, as compared to that in bulk.

As discussed above, for conventional polymers the mobility reduction,  $RF$  in porous media will, at low and moderate shear rates, be close to the relative viscosity. As demonstrated in Åsen et al. (2021) (Paper 3), Reichenbach-Klinke et al. (2016) and Leblanc et al. (2015), for associative polymers the mobility reduction in porous media will be much larger than the viscosity of the bulk solution would suggest.

Reichenbach-Klinke et al. (2016) reported a mobility reduction,  $RF$  of over 1000 at a shear rate of  $10\text{s}^{-1}$  at  $60^\circ\text{C}$  for a thermo-thickening associative polymer with a relative viscosity of less than 10 at the same shear rate.

At shear rates below the critical shear rate for onset of shear-thickening,  $RF$  for TAPs is strongly shear-thinning. Reichenbach-Klinke et al. (2016) reported that they could vary flow rates over two order of magnitude, with virtually no change in the measured differential pressure, clearly demonstrating the strong shear-thinning of  $RF$ . A similar trend is reported in Åsen et al. (2021) (Paper 3) where both our data and the data from Reichenbach-Klinke et al. (2016) are fitted to the following equation with  $\omega = 0.9$  and  $\omega = 0.95$ , respectively:

$$RF = A\dot{\gamma}^{-\omega} + RF_{\infty}. \quad (40)$$

At high shear rates, TAPs will display the shear-thickening and mechanical degradation behaviour of a regular polymer of the same molecular weight and primary composition.

So why is a much higher concentration of polymer needed in bulk to detect association than what is needed in the porous media? One explanation can be

that certain segments of the polymer solution enriched with associating moieties are retained in the porous media, so the resistance to flow is caused by a “concentrate of association”. This theory is supported by the delay in the build-up of the resistance to flow described by Reichenbach-Klinke et al. (2016); Reichenbach-Klinke et al. (2018) and which is also reported in Åsen et al. (2021) (paper 3).

Another explanation for the high resistance to flow in porous media compared to in bulk, can be the ever-changing flow fields the polymer molecules encounter in the porous media. During porous media flow, the polymers will constantly change their conformation as they are subjected to shear- and elongational flow, when the solution is accelerated thorough narrow pores, meets interconnecting flow stream and changes direction. This will stretch and elongate the molecules, exposing the hydrophobic segment to come into contact with segments on neighbouring polymers. The need for deformation of the polymers to favour intermolecular association was also noted by Seright et al. (2011). If reversible intermolecular association is dominant, the solution will obtain the flow behaviour of a dynamic weakly cross-linked gel, where force is constantly needed to break the bonds to move the fluids and new bonds are constantly being formed as they are exposed to each other. Whereas in bulk, even at shear flow, the polymers could for the most coil up on themselves, forming intramolecular interactions or stick to the same neighbouring polymer.

### **3 Experimental; methods and materials**

The primary variables quantified in this work were the volumetric flow rates,  $Q$  and the corresponding differential pressures,  $\Delta P$  across porous media, capillary tubes and other devices, which in combination with fixed properties i.e. dimensions, permeability and porosity of the porous media and dimensions of the pipes (capillary tubes, small lab-tubes and field scale pressure reducers) provide the derivable quantities, mobility reduction, see Equation (32) and shear rate, see Equations (25), (29) and (37). Mobility reduction and shear rate, together with bulk viscosity measurements of injected and produced solutions, are utilized to describe the polymer solutions' mechanical degradation and ability to reduce mobility.

The methods used in this work answers important questions about the polymer solutions' potential EOR contribution. And although the basic principles of our tests are, and have been common practice in our lab, (and several others research labs) for years, some features of our testing can be considered original: The innovative way a relative standard set-up was modified to study length effects in Paper 1 (Åsen et al., 2019), the testing at large scale and matching it to lab-scale experiments in Paper 2 (Stavland et al., 2021), and the modification of the set-up to study the effect of temperature gradient for thermo-thickening polymers in Paper 3 (Åsen et al., 2021).

That be said, the methods chosen carries the trade of Maslow's hammer ("If all you have is a hammer, everything looks like a nail"), and needs to be complimented by modelling. The porous media core is a linear, relative homogenous "black box". Core scale modelling of the results, upscaled to reservoir model is needed to understand the impact of e.g., radial flow, fracture flow, heterogeneities etc. And although the analogies presented above can provide some sense of insight to the polymer behaviour in the pores, pore scale modelling is needed to understand the exact mechanisms resulting in the overall polymer behaviour. All these types of modelling are performed by other projects in the National IOR Centre of Norway (Lohne et al., 2017; Nødland et al., 2019; Palmer et al., 2018). In addition, being able to actual visualize polymer behaviour in micromodels is desirable, for a more complete understanding.

### **3.1 Water composition**

For oil recovery experiments in porous media, one will usually need two types of water. One water representing the water in the reservoir and one representing the available injection water. Since polymer flooding is rarely performed in secondary mode, we have used the same water composition for both, that is, the porous media cores are saturated, and permeability and base line differential pressure,  $\Delta P_w$  are established with the same water composition as the polymer solutions are prepared in. For offshore implementation, the available mixing water will be produced water or sea water. We have used compositions with the same salinity as seawater, with a representative selection of ions. In the tests with the conventional polymers, a synthetic sea water (SSW) with almost all the ions present in real sea water was used, except for the problematic trace elements. For the test with the thermo-thickening polymers, a simplified synthetic sea water (SSSW) with only  $\text{Na}^+$ ,  $\text{Ca}^{2+}$  and  $\text{Cl}^-$  was used (with the same total dissolved salt (TDS) by weight and same divalent content in mol). Knowing that the conventional synthetic polymers are adversely influenced by salt, the tests with these polymers were also performed with a low salinity water with a small amount of NaCl, to gain some insight into whether the advantages of using a low salinity water might outweigh the disadvantages, i.e. costs of importing water or desalinating the available water. For a complete assessment of this, the low salinity EOR potential must also be taken into account (Smalley et al., 2018). Assuming (correctly) that the thermo-thickening polymers would be positively influenced by salt, a salt water (3xSSSW) with 3 times the salt-concentration of the simplified sea water, was used in one of the tests with these polymers. The recipes for the salt waters used are shown in Table 1.

*Experimental; methods and materials*

Table 1 The recipes for the salt waters

<b>Salt</b>	<b>SSW [g/dm<sup>3</sup>]</b>	<b>0.5% NaCl [g/dm<sup>3</sup>]</b>	<b>1.0% NaCl [g/dm<sup>3</sup>]</b>	<b>SSSW [g/dm<sup>3</sup>]</b>	<b>3xSSSW [g/dm<sup>3</sup>]</b>
NaCl	23.38	5.01	10.06	28.00	84.00
MgCl <sub>2</sub> · 6H <sub>2</sub> O	9.15				
CaCl <sub>2</sub> · 2H <sub>2</sub> O	1.91			8.00	24.00
KCl	0.75				
Na <sub>2</sub> SO <sub>4</sub>	3.41				
NaHCO <sub>3</sub>	0.168				

The salt waters mixed in the laboratory were all made from p.a. quality salts and deionized water. The water was deionized by ELGA Purelab-R7/15 water purifying system to a resistance of 15 M $\Omega$  (the higher the resistance, the lower is the content of ions). For selected tests, the oxygen content was reduced. For the large-scale tests, the tests performed outside in the yard, described in Stavland et al. (2021) (Paper 2), the NaCl-water was made from a lower grade salt, presumably drilling mud quality and from Ullrigg test Centre's fire water (stored tap water).

In the laboratory, the salt waters were mixed in volumetric flasks on a magnet stirrer. Prior to use, both the flask and the magnet were subjected to a cautionary rinse with deionized water. Usually, 5-liter flasks were used since that is the size of the filtration unit. Before adding the salts, the flask was partly filled with water, and set to stir. The salts were weight within +/-0.01 g of the recipe and added to the flask, via a funnel, one by one. The funnel and weighing boat were rinsed of with deionized water from Wash bottle into the flask, to avoid loss. As the solubility of Na<sub>2</sub>SO<sub>4</sub> increases with increasing salinity, Na<sub>2</sub>SO<sub>4</sub> was added after most of the other salts were added. Then, water was added to almost the target volume and the solution set to stir till it was clear, before NaHCO<sub>3</sub>

was added. When all the salts were added, the solution was set to stir for approximately 30 minutes, before the magnet was pulled up by an external magnet (outside the flask) to over the water/air interface and water was added to target volume. After a few minutes of additional stirring, the water was filtered through a 0.45- $\mu\text{m}$  Milipore filter, by a vacuum-filtration system, see Figure 14.



Figure 14 Vacuum-filtration system.

For some of the tests, the salt waters were purged with nitrogen via a sintered glass distribution head immersed in the fluid during stirring on a magnet stirrer, until the water had stable pH (5-6 hours). In addition, for selected tests in Åsen et al. (2019) (Paper 1), oxygen scavengers in the form of 50 ppm  $\text{Na}_2\text{SO}_3$  and 50 ppm  $\text{NaSCN}$  was added. Purging and/or adding scavengers were done to

reduce the oxygen content, as oxygen can induce chemical degradation of synthetic polymers (Gathier et al., 2020; Seright & Skjevraak, 2015). In the experiments with TAPs, oxygen scavengers were not used, as it is suspected that they are harmful to these types of polymer solutions. Purging with nitrogen was performed in all the TAP experiments.

Water pressure drops,  $\Delta P_w(T)$  across cores and capillary tubes are estimated by Equation (41),

$$\frac{\Delta P_w(20^\circ C)}{\Delta P_w(T)} = \frac{\eta_w(20^\circ C)}{\eta_w(T)}. \quad (41)$$

We estimated the viscosity of polymer solutions at elevated temperature,  $\eta_p(T)$  by using Equation (42) (i.e. assuming constant relative viscosity)

$$\eta_r = \text{const} = \frac{\eta_p(20^\circ C)}{\eta_w(20^\circ C)} = \frac{\eta_p(T)}{\eta_w(T)}. \quad (42)$$

$\Delta P_w(20^\circ C)$  is measured in the flooding rig,  $\eta_p(20^\circ C)$  is measured on the rheometer, and  $\eta_w(20^\circ C)$  and  $\eta_w(T)$  are calculated using in-house software. The viscosities of the salt waters used as a function of temperature is shown in Figure 15.

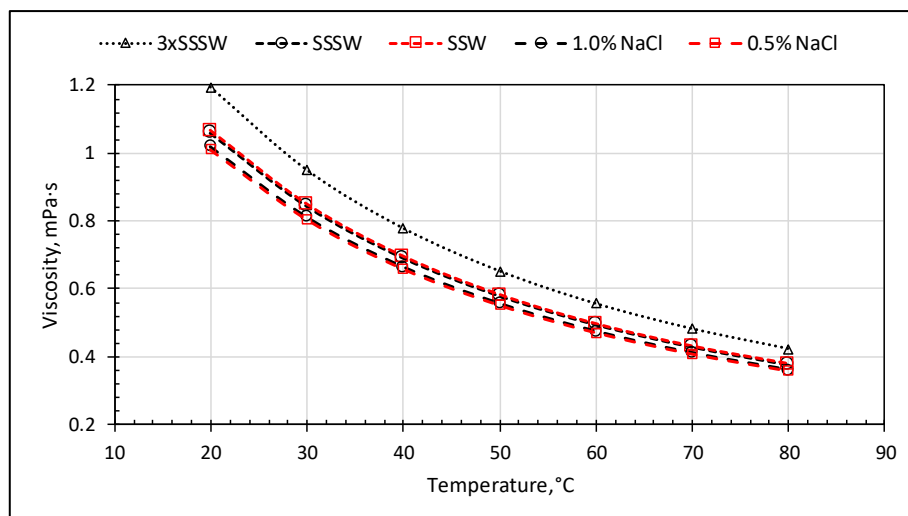


Figure 15 Calculated viscosity as a function of temperature for the salt waters.

### 3.2 Polymer solutions

The polymers studied in this work and some of their key properties are listed in Table 2. The molecular weight and composition are received from the suppliers; SNF (the regular polymers) and BASF (the thermo-thickenings associative polymer, TAPs).

Intrinsic viscosity is calculated from Equation (22), according to the method described in 2.2. When transforming the polymer concentration from ppm to  $\text{g}/\text{cm}^3$ , the density of the solution is for simplicity assumed to be  $1 \text{ g}/\text{cm}^3$ .

Table 2 Polymer properties

Polymer	Polymer type	Molecular weight	Hydrolyzation degree	ATBS degree	Relative. ass cont.	Intrinsic viscosity, $\text{cm}^3/\text{g}$		
						0.5% NaCl	(S)SS W	3xSS SW
3630	HPAM	20	30	0	-	5500	3120	-
3330	HPAM	8	30	0	-	4080	2040	-
5115	ATBS	15	30	15	-	4100	2780	-
AN125	ATBS	8	0	25	-	3230	1850	-
A06	TAP	5-8	0	25	0.6	-	1490	-
A08	TAP	5-8	0	25	0.8	-	1570	-
A10	TAP	5-8	0	25	1.0	-	1600	1558

From the values listed in Table 2 and the chemical composition of the monomers, theoretical values for number of monomers, contour length, radius of gyration at  $\theta$ -condition and residual resistance factor for one monolayer of adsorbed polymer coils can be calculated from Equations (4), (7), (9), (12), and (36), respectively. Values listed in Table 3 are calculated assuming that the cations of the acrylate and ATBS are balanced by sodium ions, that is, the molecular weight of the charged monomer units include the atomic weight of sodium. As the exact chemical structure of the TAPs are not known, these values are even more approximate than for the traditional polymers.

Table 3 Calculated values of dimensions for the polymers used in this work at theta ( $\theta$ )-conditions. Note that the three last columns are calculated assuming that the monomer unit are the freely joint segments.

Polymer	Polymer type	Average MW	Number of monomer units	Contour length	$R_{gsaw} @ \theta$ -condition	$V_{chain}/V_{coil} @ \theta$ -condition	RRF @ $R_{pm} = 10 \mu m$
		Monomers Dalton	x1000	$\mu m$	$\mu m$	ppm	-
3630	HPAM	78.0	257	65	0.14	220	1.12
3330	HPAM	78.0	103	26	0.08	460	1.07
5115	ATBS	112.4	134	35	0.09	373	1.08
AN125	ATBS	128.4	62	16	0.06	686	1.05
A06	TAP	~128	~39-62	~10-16	~0.05	1000	1.04
A08	TAP	“	“	“	“	“	“
A10	TAP	“	“	“	“	“	“

The to-be-used polymer solutions were prepared from pre-made (5 000, 10 000ppm or 15 000 ppm) stock solution. The polymers were declared to have an active content of 90%, and this was corrected for when preparing the stock solution, so that the stated concentration is active concentration.

The stock-solutions were prepared in 0.5 litre or 1 litre batches in 1 litre bottles or 2 litre plastic beakers, for the TAPs and regular polymers, respectively. The polymer powder was gradually sprinkling in-to the vortex of the salt water being stirred with a T-mixer (tip-to-tip length of 6 cm) on a Heidolph RZR 2021-mixer rotating at 300 rpm for the TAP and 700 rpm for the regular polymers. Gradually sprinkling in essential, as adding the polymer powder too fast can cause polymer corns to stick to each other and not be properly hydrated (aka “fish-eyes”), and too slow can give a viscous solution before all is stirred in, leading to inadequate mixing.

For the TAPs, mixing commenced for 0.5 hours at 300 rpm, before the speed was lowered to 200 rpm, and mixing and hydration commenced overnight. During mixing, the solution was covered with caps with holes for the mixer rod. After mixing, the solutions were covered with a nitrogen blanketed, capped, and stored in a refrigerator pending preparation of the diluted solutions.

For the regular polymers, mixing at 700 rpm commenced for 1 hour, before mixing continued for 2 hours at 300 rpm, where-after hydration and further mixing was performed on a magnet stirrer overnight. If the stock-solutions were not to be used immediately, they were stored in a refrigerator under a nitrogen blanket.

The diluted solutions were mixed just prior to use, from stock solution and salt water, on a magnet stirrer for at least 0.5 hours. For the TAPs, the solutions were prepared in oxygen reduced water and during stirring, the solutions were purged with pure nitrogen and covered with para-film. Due to the amphiphilic nature of the associative polymer, foam was generated during purging. It is therefore important to supervise the solution and keep the rate of nitrogen gas low, to avoid foam overflow.

For all the diluted polymer solutions, the viscosity as a function of shear rate was measured at 20°C by a cone and plate geometry on an Anton Paar MCR301 Rheometer. The sample size used for that set-up was 3.95 ml. The sample was usually transferred by a 5 ml Finnpiptette (from Thermo Scientific), but for the most viscous solution, 5 ml graded single use syringes (Norm-jet from HenkeSassWolf) were used, because the syringes disadvantage; reduction in volume measurement precision, was outweighed by the advantage of actually getting all of the viscous sample out of the syringe.

The viscosity was typically measured from 0.1-500 s<sup>-1</sup> and 500-0.1 s<sup>-1</sup>, referred to as up and down, with a logarithmic distribution on the shear rate scale of 40 measuring points (20 up and 20 down). The measuring points had a fixed duration of 10 seconds, so the time for one scan was a little under 7 min, not including loading of the sample, positioning the cone, and rinsing of plate and cone. The gap between cone and plate was 0.052 mm, and gap was adjusted daily, by the set zero gap command of the software. This must be set at the temperature at which the measurements are performed, to avoid discrepancy

between the set gap and the actual gap, with ensuing miscalculation of the viscosity, due to thermal expansion of the equipment. Although of no concern in this work, it might be worth sharing that Anton Paar recommend that for a temperature scan, the zero gap should be set for the temperature in the middle of the temperature range. Motor adjustments, also a command of the software, was performed routinely, every 90 days or when the low shear rate measurements, (usually of low viscosity samples), became fuzzy. For high viscosity samples, typical for the stock solutions, shear scans could only be performed up to  $130 \text{ s}^{-1}$  ( $2 \times 17$  measuring points). At higher shear rates, the sample would escape by creeping up on the plate, due to the normal force displayed by viscoelastic solution. This phenomenon is the same as the rod climbing Weissenberg effect observed during mixing of polymer solutions, where the solutions creep upwards on the mixing rod, creating a cone like shape around the rod. Watching the sample escape the gap between the cone and the plate is quite a thing to behold. Contrary to what one might imagine, and what will probably happen to very low viscous fluid at high rotation speed, the fluid is not slinged outwards by the centrifugal effect, but rather creeps over the edge of the cone and (if memory serves right) in towards the rod.

For the degradation experiments, the viscosity of effluent samples was measured as described for the initial solutions. And degradation was calculated according to Equation (39). The samples were collected at stable conditions (stable differential pressure), and samples of at least 6 ml were collected for each measuring point/pumping rate. For the large-scale tests, larger samples were collected (~0.5- 1 litre), and some of them were subjected to additional testing in other projects.

For the tests performed with the TAPs, only the initial solutions viscosity was measured by the above-described procedure on the rheometer. For these tests, the effluent viscosity was measured by in-line viscometers in the form of capillary tubes with pressure transmitters. There are several reasons for this. Firstly, the in-line viscometers are superior to the sampling-method when it comes to detecting breakthrough of polymer since it is located immediately after the cores and only a small amount of polymer solution (0.8 ml) is needed to fill the tube and read an instant response from the pressure transmitter. Secondly, since the tests with thermo-thickening polymers naturally has to be performed at elevated temperature, a backpressure had to be applied to avoid

gas bubbles forming. Passing through the backpressure regulator will severely degrade the polymer, rendering viscosity measurements of the effluent after passing the regulator pointless. Thirdly, we don't expect mechanical degradation of the TAPs at the prevailing test conditions, but if there were, this would have been detected qualitatively (Not quantitatively as the viscosity is only measured at the prevailing shear rate).

### **3.3 Core mounting and sand packing**

In two of the papers produced from this work, the polymer solutions were assessed by flooding through cylindrical porous media cores. The length and, on one occasion, the diameter of the cores varied. Bentheimer cores were used to measure mechanical degradation as a function of length (Åsen et al., 2019). Bentheimer, Berea and unconsolidated sand were used to evaluate the flow behaviour of TAPs. (Åsen et al., 2021). All the studies were performed at 100% water saturation.

Bentheimer and Berea are both outcrop rocks frequently used as model porous media for studying non-field-specific flow in petroleum reservoir rock. Outcrop rocks are usually easier to handle, more available and with less variation in properties from sample to sample compared to actual reservoir rock. The outcrop rocks are usually bought in blocks and cores are drilled out at an in-house work-shop (see Figure 16) to standard diameters (most frequently 1.5 inch/3.8 cm) and maximum achievable length (30 cm or 1m), and are cut to desired length by a Struers Labotom-5 saw prior to use.



Figure 16 Cores being drilled out of a 40cmx40cmx30 cm block by Ronny Håland, UTC. (Photo: Ronny Håland).

The unconsolidated sand was supplied by Covia Europe and is a >99% pure 100 mesh quartz sand. The sand yields a permeability,  $k_{50bar}$  of ~8 Darcy with 50 bar overburden pressure and,  $k_{0bar}$  of ~12 Darcy without overburden pressure, and porosity,  $\varphi$  of ~0.33 with overburden and ~0.35 without overburden. The porosity decreases because the overburden pressure pushes the sand grains closer together, and the decrease in porosity will according to Carman-Kozeny, Equation (38), also impact the permeability. Presumably, the particle size,  $D_p$  will not be changed by applying overburden pressure. Neglecting the tortuosity,  $\tau$ , the impact of the porosity change on the permeability will be:

$$\frac{k_{0bar}}{k_{50bar}} = \left(\frac{\varphi_{0bar}}{\varphi_{50bar}}\right)^3 \left(\frac{1-\varphi_{50bar}}{1-\varphi_{0bar}}\right)^2. \quad (43)$$

For a porosity without overburden,  $\varphi_{0bar}$  of 0.35 and porosity with,  $\varphi_{50bar}$  of 0.33, the permeability without overburden,  $k_{0bar}$  will be  $1.26 \cdot k_{50bar}$ , the permeability with overburden. This is a little lower than the measured values, possibly because the improved packing with overburden will also impact the tortuosity, as more pore throats will be cut-off and the solution will have to travel and even longer way around. Simply put, the tortuosity is the ratio between the length of the detour the solution must travel due to obstacles to the straight-line distance. That be said, the calculation is also very sensitive to the precision of the porosity values. If the values are in fact 0.354 at 50 bar and 0.325 at 0 bar,  $k_{0bar}$  will be  $1.4k_{50bar}$ , close to the measured of 1.5.

Mounting dry consolidated sandstone cores like Berea and Bentheimer in core-holders is relatively straight forward. The pieces of the core holders can be seen in Figure 17. The core is pushed into the rubber sleeve. The end-piece, which is floating on the tubing, is inserted, and affixed with a copper or steel string to the rubber sleeve. Then the outer metal sleeve is screwed onto the in-side tread of the end-piece. The second end-piece (fixed) is then connected to the rubber sleeve with a copper or steel string, and the fixed end piece is thereafter screwed onto the outer steel sleeve. The floating endpiece is thereafter unscrewed and overburden oil (Marcol) is introduced in the compartment between the rubber sleeve and the outer steel sleeve, with the core holder in vertical position. The core holder is kept in vertical position by placing it in a swivel bench vice. After re-tightening the floating endpiece to the outer sleeve, with the overburden

valve open to push out all air, additional overburden oil is pumped into the oil compartment to the desired overburden pressure via the overburden valve.

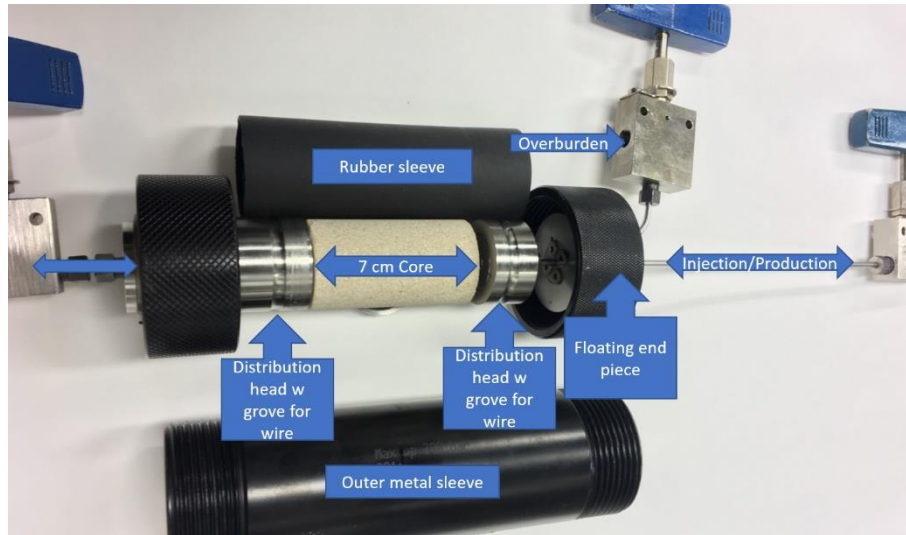


Figure 17 The pieces of the core holder.

For the sand packs in core holders, the principle is essential the same, but the process is significantly more cumbersome, as the sleeve must be mounted on the floating endpiece before introducing the sand, and the sleeve has to remain vertically during the packing. To avoid sand migrating out of the tubes, screens must be used. In this work, thin slices (~0.5 cm) of Bentheimer were mounted on each side of the sand-pack. While dry sand was introduced slowly to the rubber sleeve via a funnel, a hammer was used to knock on the rubber sleeve and the endpiece, to ensure satisfactory packing. When knocking no-longer compacts the sand (the height of the sand in the rubber sleeve was constant), all sand grains on the inside of the rubber sleeve that will be in contact with the end-piece was removed to avoid leakage between the oil compartment and the core. Thereafter overburden oil and pressure was applied as for the consolidated cores.

When we packed the sand in a steel cylinder without overburden pressure, dry sand was introduced steadily to the cylinder during constant knocking with a hammer. Hearing protections is recommended. When the steel tube was almost filled, the second end-piece was partly screwed on, and knocking continues,

entailing improved packing, so the end-piece can be screwed further down, and more sand can be added. This was repeated until knocking no longer brought about further compaction.

After mounting the cores or sand in the core holders, or packing the sand in the steel tube, the porous media is evacuated with a vacuum pump (Two Stage High Vacuum Pump by Edwards High Vacuum), and salt water is introduced from a Quizix-pump (Model: QX6000HC-SPR-195) with accurate volume control to measure pore volume of the porous media. Practically, this is done by filling the tubing to the in-let valve of the core holder with the water, connect the tubing to the core holder, and pump the system (pump, tubing and usually piston cell) up to the in-let valve to desired pore pressure, by setting the safety pressure on the pump to said pressure. Then the valve to the core is carefully opened, cumulative volume of the pump reset to zero, and the pump is set to pump at a medium rate (5-10 ml/min), until desired pore pressure is reached, and pump stops due to safety pressure reached. If the pressure decreases, which is often the case for tighter rocks than the once used in this work, the injection till reaching safety pressure is repeated a couple of times, before cumulative pump volume is recorded and the dead volume of the core holder is subtracted to get the pore volume of the core. The dead volume of the standard core holders used in this work (in-house FB core holder for cores of 3-12 cm and diameter of ~3.8 cm) is 1.16-1.18 ml and is the volume of the distribution heads, closed valves, and steel tubes. The porosity is the pore volume divided by the core's bulk volume. The bulk volume is given by the diameter and length of the cylindrical core measured by a caliper prior to mounting it in the core holder. The pore volume is also quality assured by weighing the core holder before and after introducing the water.

After installing the core holders or steel cylinder in their flooding-rigs, salt water is injected at multiple rates, to measure permeability and, when applicable, get base line pressure drops for the capillary tubes. The same pump and salt water that was used to measure pore volume is used. As the salt waters' viscosities are known across the temperature range of the tests, absolute permeability and capillary tube-baselines are only measured at 20°C. In the flooding rigs, the overburden compartments of the core holders are connected to an external pressure source, that is a piston cell at room temperature with overburden oil (Marcol) on the side connected to the core holder and

pressurized nitrogen gas connected to a manometer on the other side of the piston. This is especially important when the core holders are heated to avoid overburden pressure increase but is also used at ambient condition to avoid loss of overburden pressure. The overburden pressure is set above the injection pressure to ensure matrix flow, that is; avoid flow between the core and the rubber sleeve.

### **3.4 Flooding rigs and set-ups**

Generally, the flooding rigs used in this work are set up with all the necessary equipment to maintain desired conditions and measure chosen parameters when pumping fluids through a device or a porous media core. The flow behaviour has been studied in porous media, capillary tubes and steel pipe of different dimensions, and choke valves. “Desired conditions” are the back pressure (pore pressure), overburden pressure and temperature. The back pressure and temperature were for most of our tests set to ambient, and for the rest are controlled by placing the device in heating cabinets with back pressure regulator and overburden pressure cell placed at room temperature. The injection rate is measured and controlled by pumps, and the resulting differential pressure is measured, except for the test with the mm-scale (id=1.75 mm) steel pipes in Stavland et al. (2021), where the injection pressure is controlled, and the resulting injection rate is measured. Differential pressure is usually measured by differential pressure transmitters (Fuji and Honeywell transmitters) but has also been stipulated from injection pressure minus back pressure. This is usually done when the differential pressure is too high for the pressure transmitter to measure it, where will also be where the injection pressure is high and small fluctuations or uncertainties in back pressure (whether set by back pressure regulator or atmospheric pressure) will not contribute to the overall results.

In Åsen et al. (2019) the main objective was to measure degradation as a function of length travelled by the polymer solution in the porous media at different volumetric injection rates. To that end, a flooding rig with 4 core holders in series, each with its own pressure transmitter and designated by-pass lines was constructed. A 30 cm long Bentheimer core (3.8 cm in diameter) was cut into four segments of 3, 5, 8 and 13 cm. The missing centimetre is unavoidable loss caused by the saw. The core holders were placed in series according to increasing length. This is because we strongly suspect that any

length effect on degradation will be most severe in the first few centimetre and then decline, so measuring points can be further apart. A sketch of the set-up, is shown in Figure 18

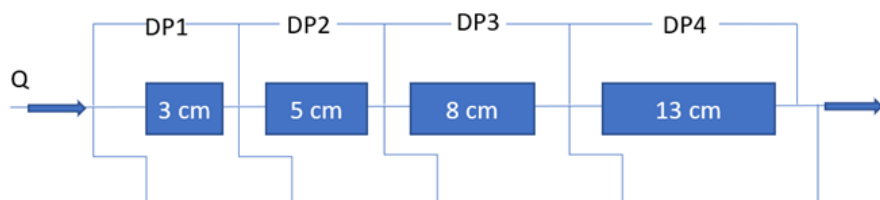


Figure 18 Flooding rig for studying length effects.

Courtesy of the designated by-pass line, effluent samples could be collected after injection through by-pass only, 3 cm, 3+5 cm, 3+5+8 cm and 3+5+8+21 cm, but also through only the full 8 cm or 13 cm. And due to the choice of length take from the Fibonacci sequence, the set-up could be used to test if the introduction of additional entrance surfaces would influence mechanical degradation. That is, test if injecting through 3+5 cm (or 5+8) would yield a different degradation and mobility reduction as compared to injecting through the full 8 cm (or 13 cm). The example in brackets was planned, but due to an incuria not performed.

Incidentally, to avoid using too much polymer solution and time, the set-up had to be operated by 3 people, Daniel Strand, Arne Stavland and this candidate; one operating the pump (notify when stable differential pressure was reached so that effluent samples could be collected and change injection rate), one operating the valves, so the correct core length was flooded, and one collecting the effluent samples. Injection rates of up to 98 ml/min was used. This was achieved by using two pumps in parallel with maximum injection rate of 50 ml/min. Because of the high injection rate, long core length and shear-thickening nature of the polymer, the injection pressure would on occasions be so high that the overburden pressure had to be increased to up to 130 bar.

Modified versions of this set-up were also used for two additional purposes. First, to evaluate degradation as a function of length up to 20 meters by recycling polymer solution at fixed rates. And secondly, evaluated the effect of

radial flow, by re-injecting polymer degraded at high rates (corresponding to near well area rates), at lower rates (corresponding to in-depth propagation).

In Stavland et al. (2021), polymer degradation was studied across scales, and correspondingly the set-ups used varied.

At the smallest scale, degradation was measured in capillary tubes (internal diameter (id) down to 0.127 mm). The capillary tubes were cut to desired length by a special cutting device supplied from the vendor of the capillary tubes designed to avoid squeezing the tubes and changing the dimension and shape of the tube. After cutting, the tubes were inspected under a microscope to ensure that the opening was circular and not damaged. The length was measured by a digital caliper. In the set-up, the inlet of the set-up (capillary tube and steel tube) was connected to a differential pressure transmitter and the polymer reservoir via a three-way coupling. The outlet of the capillary tube and the low-pressure side of the pressure transmitter were both open to atmospheric pressure. Caution had to be taken when the bypass of the pressure transmitter was open, to avoid that fluid poured out due to the open capillary tube. Effluent fractions for analyses were sampled directly from the outlet of the capillary tube.

At the medium scale (mm-scale) degradation was measured in a steel pipe (id=1.75 mm), the same kind of pipe usually used to connect the equipment in our flooding rigs. These experiments were performed to close the gap between the laminar flow prevailing at all injection rates in the capillary tubes, and the turbulent flow encountered in the large-scale tests. This set-up was very much ad-hoc. The steel pipe was connected to a piston cell, with a large outlet via a connector with ~twice the diameter of the steel pipe, with a “binary” valve (opens by turning 45°) between the connector and the pipe. The entire set-up was mounted horizontal without any bends. The piston cell was filled with ~0.5 litres of polymer solution and the back-end was connected to a nitrogen pressure tank. The pressure tank and piston cell were pressurized to desired injection pressure by the pressure tank’s regulator. When the valve was opened, the polymer solution was pushed through the steel tube and was collected in a plastic bottle with a self-made hole for the pipe. The plastic bottle was placed on a scale, and the scale was filmed with a cell phone camera. The flow rate was calculated by visual inspection of the film, from the time stamps on the

film and the digit on the scale. One filling of the piston cell gave one measuring point of effluent viscosity as a function of rate and differential pressure.

At large scale, the devices tested, and equipment used were mostly operated by personal from Halliburton. The devices tested where two commercial adjustable choke valves (one at a time), two fixed chokes (orifices with a fixed id, smaller than the id of the main pipes), a linear pressure reduced (a very long steel pipe where the pressure drop was adjusted by varying length or flow rate), and serial mounted adjustable choke valves (3 at a time). The set-up was installed in the Yard, out-door at Ullrigg test Centre at Ullandhaug, just outside our lab where measurements on the polymer solutions and effluent samples were performed. Disregarding the size of the equipment involved and the volume of the solutions mixed, the main difference between this set-up and the set-ups otherwise used was the way the differential pressure was attained, and the way polymer samples were collected. The pressure was measured by pressure transmitters installed on each side of the device, and differential pressure was calculated, not measured directly. Polymer samples were collected on-line by special low shear sampling devices installed up-front and downstream of the tested device. As there was some mechanical degradation during mixing and pumping, degradation was determined by the difference in viscosity of the sample taken up-front the device and the sample taken down stream. The SNF-sampling devices were operated by personnel from SNF.

Two different set-ups (flooding rigs) were designed for evaluating the flow behaviour of the thermo-thickening associative polymers (Åsen et al., 2021).

In the first set-up, three cylindrical cores of approximately the same dimension (7 cm long, 3.8 cm wide) were mounted in individual core holders. Although 3 types of porous medias were used, the same type of porous media was used in the same test. That is, no tests were performed with different porous media at the same time in the three core holders. Overburden pressure of 50 bar was applied. The core holders were coupled in series, each placed at a different temperature. That is, the first core holder was placed on the bench and the two following were placed in two different heating cabinets, each at a higher temperature than the preceding core (injection from low to high temperature to mimic a reservoir with temperature gradient). Each core holder was connected to two differential pressure transmitters; one with a narrow range and high

resolution for the pressure drops expected during water injection and for non-associative polymer flow, and one with a broad range and correspondingly low resolution, for the high differential pressure expected during thermo-thickening. Capillary tubes (CT) with differential pressure transmitters were used as in-line viscometers to monitor polymer break through (and potential degradation, which was not observed). The capillary tubes were placed on each side of the three core holders. A sketch of the set-up can be viewed in Figure 19. As the experiments were performed at elevated temperature, a back-pressure regulator set to 10 bar was applied.

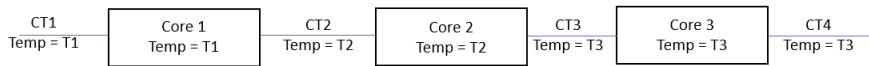


Figure 19 Sketch of the experimental set-up/flooding rig with 3 cores and capillary tubes (CT) in series. The injection direction is from left to right, from low to high temperature. T1 was 20°C in all the experiments. T2 was 60°C and T3 was 80°C, in all but the first experiment (Experiment 1a), where they were 30°C and 60°C, respectively.

To investigate how thermo-thickening scales with spatial dimensions, a set-up (see Figure 20) with a longer ( $l=76$  cm) and wider ( $d=5.36$  cm) cylindrical porous media was used. A steel cylinder with pressure ports, enabling differential pressure readings over four equally spaced sections, was, as previously described in detail, packed with unconsolidated sand, and placed vertically in a heating cabinet. As for the smaller scale thermo-thickening test, two differential pressure transmitters were used for each of the four sections, in-line viscometers were placed on each side of the steel cylinder and back pressure of 10 bar was applied.

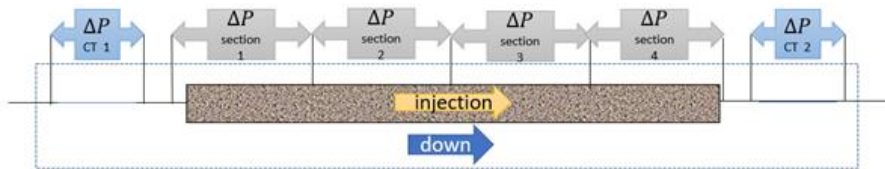


Figure 20 Sketch of the experimental set-up (flooding rig) with a 76 cm long sand pack in a steel cylinder used in Experiment 7 to 9. The dashed blue rectangle shows what is inside the heating cabinet. The blue lines show the capillary tubes (CT).

As previously noted, back-pressure regulator (BPR) will severely degrade polymer solutions. This is an unavoidable consequence of the design of our in-house BPR. A membrane is pushed onto a surface between the inlet and outlet of the regulator by a pressurized gas. When the fluid has the same pressure as the pressurized gas, it is squeezed through a narrow opening between the membrane and the surface, and this squeezing has proven detrimental to the viscosity of polymer solutions. Another challenge with the BPR, is the relatively small amount of pressurized gas above the membrane. If the temperature of the gas is changed e.g., by a change of the volumetric rate of the heated effluent fluid (or production of gas that will expand and cool the BPR), the pressure in the pressurized compartment will change, and the back pressure will fluctuate. In this work the latter problem has been reduced by connecting the pressurized compartment to larger N<sub>2</sub>-pressurized cell (a 2-liter piston cell without a piston). If the fluctuation is caused by gas production inducing cooling, the above-mentioned solution can also apply, but heating the BPR by for instance a heating coil, will also give some relief.

## **4 Results: Key findings and Discussion**

Two important success criteria to obtain accelerated oil production and reduced (delayed) water production is significant in-depth mobility reduction, and, at the same time, maintain reasonable injectivity. For regular synthetic polymers, mobility reduction is strongly linked to a viscosity increase which is usually negatively affected by salinity. A further challenge with synthetic polymers is mechanical degradation, which is chain cleavage of the polymer backbone. Mechanical degradation can be an issue in all handling of polymer solutions where the polymer molecules can be exposed to shear or elongational forces. To avoid degradation special pumps must be used and care must be taken during mixing. The pressure drop in chokes can also be damaging. And it is suspected that turbulent flow may degrade the solution during transport (Karami et al., 2018; Kim et al., 2000). According to Jouenne et al. (2015) it is a rule of thumb in the industry that there is a limit to how far and fast polymer solution can be transported in pipes. Additionally, when it comes to evaluating mechanical degradation, the high velocities in the injection zone of the reservoir must be taken into consideration, and this is also where the shear-thickening behaviour can cause injectivity issues.

Could mechanical degradation also occur deep in the reservoir? It is suggested that mechanical degradation is restricted to the entrance of the sand face (Jouenne et al., 2018; Martin, 1986; Seright, 1983), or to a very short distance, i.e. a few centimetres into the reservoir (Maerker, 1975; Warner, 1976).

However, keeping in mind that the flow field in the porous media is very distorted and changes from point to point, one may picture that for every passing of a pore throat there is a certain probability that a polymer molecule breaks depending on where in the flow-field it passes and what transient conformation it has at this point. Some polymer molecules will have a conformation making them vulnerable to chain breaks, whereas others may have a more favourable conformation at the most critical point. And some may pass where the forces are strong, and some may pass where they are milder. Then, some of the polymer molecules may pass unharmed. And the unharmed portion of the polymers may pass at the most harmful place in the next passing of a pore throat, and so on. Then a larger and larger portion of the polymer

molecules will have been broken with number of passages. But as the number of molecules with high molecular weight will of course also decline, the rate of degradation will presumably decline with length travelled in the porous media. For reservoir with declining velocity with distance from injector, the forces that can harm the polymer molecules will also decline.

The results in this work confirm that mechanical degradation, in terms of normalized degradation, that is normalized compared to the initial viscosity and corrected for solvent viscosity as defined by Equation (39), increases with molecular weight, and that viscosity prior to degradation is reduced with increasing salinity, less for the polymers with AMPS incorporated than for HPAM without AMPS. The results also demonstrate, in compliance with Martin (1986) that salinity strongly influence mechanical degradation of HPAM, while the degradation of polymers containing AMPS is virtually the same in water with sea-water-like salinity as in low salinity NaCl-water. Going with the hair-brushing metaphor, one may say that the sulfonated appendix (see Figure 7) operates as a hair-conditioner, keeping the polymer chains apart and untangled.

When investigating mechanical degradation across scales in chokes and pipes of different dimensions, at turbulent and laminar flow (Stavland et al., 2021), it was demonstrated that degradation is not controlled by Reynolds number, velocity or pressure drop. That turbulent flow itself, at least not in the range of Reynolds number used in our tests, does not degrade the polymer, means that without additional flow constrictions in a pipe, the polymer solution can be transported over long distances. That pressure drop itself does not degrade polymer, means that polymer solutions can be injected at desired pressure if the pressure adjustment is performed adequately. Our results identified three methods for adequate pressure adjustment: Mechanical degradation during choking can be reduced by 1) increasing the length of the choke, 2) dilute the polymer solution after choking as it was found that degradation is reduced by increasing concentration, or 3) by using several standard chokes in series, each set below a critical pressure drop.

By accounting for different friction factors for laminar and turbulent flow, and accounting for the drag reducing abilities of polymers at turbulent flow, it was demonstrated the mechanical degradation scales with the shear rate. The

consequence of deducing the shear rate from the drag reducing friction factor is that the expression for shear rate at turbulent flow is, in contradiction to the laminar one, dependent on the density and viscosity of the fluid. Using the expressions for the shear rate in Equation (25) at laminar flow and Equation (29) with  $\eta_\infty = 2.5$  cP,  $\beta = 1/4$  and  $a_p = 0.155$  at turbulent flow, degradation data spanning almost 4 orders of magnitude in shear rate could be fitted to a Carreau-type model in Equation (44).  $\beta$  was set equal to the exponent in Blasius (1913) in the expression for the friction factor and  $a_p$  was found by tuning to the available data. The resulting value for  $a_p$  was in line with observed drag reduction, see Equation (28).

$$\eta_N = [1 + (\lambda_3 \dot{\gamma})^2]^{-m/2}. \quad (44)$$

Here,  $\eta_N$  is the normalized remaining viscosity, as defined by Equation (39) and  $\lambda_3$  is the critical time constant for onset of degradation, that is  $\lambda_3 = \frac{1}{\dot{\gamma}_c}$ , where  $\dot{\gamma}_c$  is the critical shear rate for on-set of degradation. Using a Carreau-type model for fitting degradation is introduced in Stavland et al. (2010), where  $\lambda_2$  is used for the critical time constant for on-set of shear-thickening in porous media.

For the investigation of distribution of mechanical degradation in porous media, the validity of dividing the 30 cm long core into individual segments and mounting them in separate core holders was confirmed. The flooding method used is illustrated in Figure 21 That is, the normalized remaining viscosity,  $\eta_N$  after injecting at the same rates, were the same when injecting through two cores of 3 and 5 cm as when injecting through one core of 8 cm, and differential pressure,  $\Delta p$  across 8 cm where the same as the sum of the differential pressure across 3 and 5 cm.

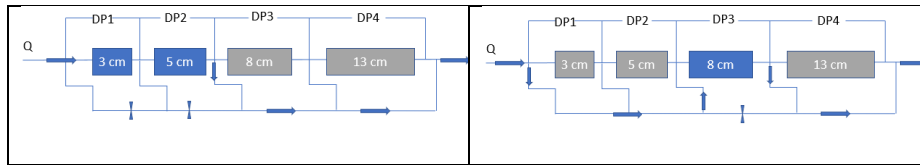


Figure 21 How the experimental set-up was used to test if introducing an extra entrance surface would influence our results.

Mechanical degradation as a function of length travelled in the porous media was measured by two different methods with length independent velocity (i.e., linear core floods) for four polymer solutions. One method where distribution of degradation was measure for a range of velocities (ranging 2 orders of magnitude) as a function of length travelled in the core, i.e., after 3 cm, 8 cm, 16 cm and 29 cm (see Figure 22, left). And one method where degradation as a function of length was measured by recycling two of the polymer solutions at two velocities up to length corresponding to 21 meters (see Figure 22, right).

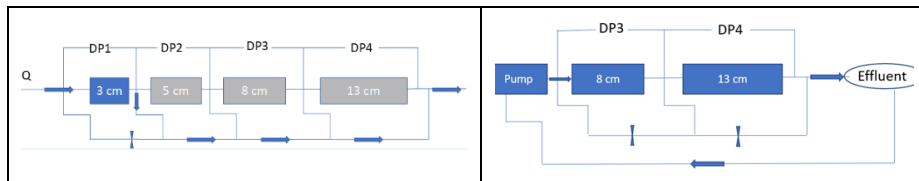


Figure 22 Modified flooding rigs.

In Åsen et al. (2019) the results are plotted in multitude of ways. The main finding is that even though the majority of the degradation happens in the first few cm of the core, at least when the velocity is high, there is declining but on-going degradation for several meters when the velocity is constant. The degradation follows a power law dependency on length, and the recycling experiments and experiments through one core length shows practically the same results. This is consistent with the consideration that for every passing of a pore throat, only a fraction of the polymer molecules will be in a “situation” where it ruptures, and the unharmed polymer molecules may be in this situation during the passing of following constrictions. This is in line with the observation made, that the higher the degradation the larger is the portion of the degradation that occurs in the first few centimetres.

But on the positive side, the length dependent degradation is not realistic at field condition. For one, it is associated with high pressure gradients (in the order of 100 bar/m) which is not realistic over long distances. Hence, the propagation rate must be lower and velocity at field conditions not linear, with correspondingly reduced degradation. For a simple radial case (see Figure 23) the velocity will be proportional to the inverse of the distance from the injector. Secondly, degradation results in lower molecular weight polymers which are less susceptible to further mechanical degradation. Figure 23, right shows the

shear rate (log-log plot) and interstitial velocity (lin-log plot) as a function of distance from the well for the properties listed in the figure insert (green text box).

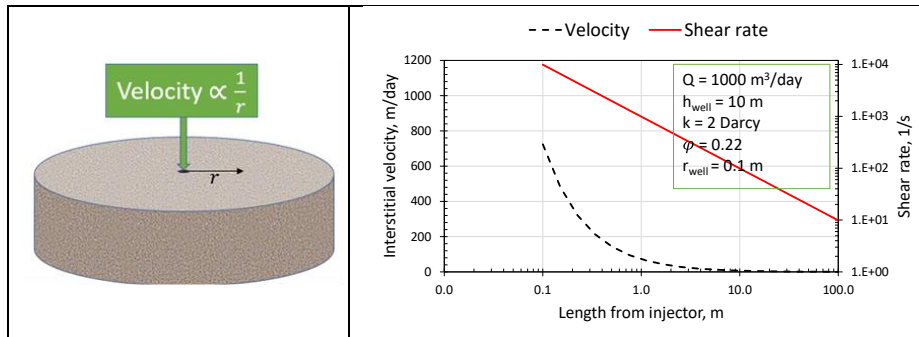


Figure 23 Radial velocity gradient.

The experiments performed to mimic a non-linear field, indicated that when the velocity declines, the degradation will be limited by the degradation at the highest velocity. This is presumably due to a combination of declining velocity and reduced molecular weight.

Drawing from the results from the multiple chokes in series and the porous media tests with re-injection of pre degraded polymer solutions, it can be hypothesized that it to some extent will be irrelevant where and when the mechanical degradation takes place, meaning that if a certain polymer solution will be degraded to 80% by a certain process, it will not degrade further if it is already degraded to 80% or less, by a process endured earlier. If this consideration is valid, alternatively one could start with a polymer product with molecular weight equal to the 80% degraded solution, which then could give the same in-depth mobility reduction.

This consideration may be said to be contradicted by the observed length effect in porous media and the consideration that only a portion of the polymer that can be degraded will be degraded for each passing. It may still be said to be valid if we consider the “certain process” completed when all the polymer molecules that can be degraded by that process has been degraded.

In terms of injectivity, some degradation will be beneficial, as degradation has a preference towards the higher molecular weight fraction of the polymer

molecules (Martin, 1986) which will contribute the most to shear-thickening (Stavland et al., 2010) and potential plugging (Seright et al., 2011).

Despite their proven success, traditional synthetic EOR-polymers have their drawbacks: High molecular weight is needed for high viscosity, low molecular weight improves mechanical stability and injectivity, viscosity is reduced by salt and temperature, and mechanical stability is also impaired by salt.

Thermo-thickening associative polymers (TAPs), on the other hand, have a thickening effect that increases with increasing temperature and salinity, is, above a critical temperature, amplified in porous media and is much higher at low shear rates compared to traditional polymers of the same molecular weight.

Since the thickening effect does not merely rely on the molecular weight, lower molecular weight polymers can be used, which will give less degradation and better injectivity. For a reservoir with a cooled down injection area, the triggering of the thickening by the in-depth temperature will of course also be beneficial in terms of injectivity.

As mentioned earlier, below a critical temperature TAPs behave as regular polymers and above they behave as hydrophobically associative polymers. The theoretical framework describing the flow behaviour of associative polymers in bulk strongly suggest that their concentration and shear rate dependent flow behaviour is dictated by the balance between inter- and intramolecular association. A high enough concentration is need for intermolecular association to be probable, a sufficient shear rate is needed for intramolecular association to be disrupted so that intermolecular association can take place, and at higher shear rate the weak hydrophobic intermolecular association is easily broken (and new ones formed) resulting in a strongly shear-thinning nature and hysteresis effects.

By investigating the behaviour of TAPs with different associative content in different types of porous media, we confirmed that the mobility reduction in porous media is strongly amplified and can be as much as 2 orders of magnitude higher than what is expected from viscosity. In an attempt to shed some light on the role of the porous media in this regard, different porous mediums were tested, but within the limited diversity of our tests, the nature of the porous

media had no significant impact on the mobility reduction as a function of shear rate.

In addition to varying the porous media, we also varied associative content, concentration, and injection rates in the experiments with temperature gradient. By some tuning it was found that the on-set of thermo-thickening for these TAPs were between 40°C and 60°C. As one would expect, increasing associative content or concentration improved the system, both with regards to magnitude of mobility reduction, reduced delay (response “time”) and stability.

The delay refers to the volume of polymer solution needed to reach stable mobility reduction. For systems at thermo-thickening conditions, we usually observed that the build-up of resistance to flow began as the polymer front entered the core, but up-to as much as 50 pore volumes of polymer solution had to be injected before the mobility reduction reached steady state. And although polymer break-through, measured by the capillary tubes, happened when expected, that is, after injecting a little over one pore volume, the build of mobility reduction in the following core (or following segment for the larger sand-pack) did not start until steady state was reached in the previous core (or segment). Accordingly, there seems to be some sort of consumption of the ability to thermo-thicken during the build-up of resistance to flow. This is supported by observations made in capillary tubes of the sand pack in the high salinity experiment. There, the system was sufficiently thermo-thickening to display weak signs of thermo-thickening in the capillary tubes as well, but only in the front capillary until stable mobility reduction was reached in the last (fourth) segment. Only then, signs of thermo-thickening were also observed in the out-let capillary tube.

Using a front core at room-temperature (below the temperature for on-set of thermo-thickening), demonstrated that the consumption of ability to thermo-thicken, fortunately did not take place when the system is not hydrophobically associating.

As stated above, the stability of the systems improved by increasing associative content. For the weaker, less stable systems, a breakdown of the resistance to flow was observed at the lowest shear rate. This is not in direct contradiction to the shear-thinning behaviour; as the shear rate was lowered, the first response

was for the mobility reduction to increase, but after some time it broke down reverting to the flow behaviour of a regular polymer solution. This is presumably attributed to formation of intramolecular association not adequately disturbed at these low shear rates to break and form new intermolecular association.

During the test in the large sand pack, we found that the investigated TAPs, equivalent to what is reported for other hydrophobically associative polymers, are positively influenced by salt. Increasing the salinity both decreased the delay, increased the magnitude of the mobility reduction, and improved the uniformity of mobility reduction.

It is still an open question what it is about the porous media flow or porous media/polymer interaction that yields the high mobility reduction compared to what is observed in capillary tube flow and expected from viscosity measurements. A better understanding of this, and what mechanisms are responsible for the delay of the build-up of the mobility reduction, is needed to understand how TAPs should be modified for optimum EOR-behaviour at reservoir conditions. Factors and mechanisms believed to be important in these regards, and for the overall “sluggish” behaviour of TAPs in porous media, are presented in the “Concluding remarks” of Paper 3 (Åsen et al., 2021). In short, the balance between adsorbed and desorption, the conformation of the adsorbed and flowing polymers, and how these (conformations and adsorption/desorption) and the inter- and intramolecular association are influenced by the complex flow field, are believed to be key aspects.

## **5 Further work**

During this work and the writing process, questions and issues related to the flow behaviour of polymer solutions have emerged. In relations to some of them, preliminary work was started, but due to lack of time or other resources, tangible results have, as of now, not been attained or processed.

At a point during the PhD work we considered to pursue experiments on micro models, but we deemed them unrealistic given the limited time available. The original plan was to do this with micro-PIV (particle image velocimetry), where the solution is seeded with micro-particles, which are expected to follow the flow field and can be tracked. This could reveal information regarding shear rates, velocity profiles, concentration gradients, depleted layer effects and potential dead (stagnant) zones.

Ideally, direct visualization of the conformation of individual polymer molecules during shear-, elongational- and complex flow would be desirable, as this would presumably disclose with certainty in what situations polymer molecules rupture. It could also be useful to know whether there is a fundamental difference in the conformation change of the polymer molecules when they are stretched by shear flow as compared to when they are elongated by elongational flow. It would also be interesting to see whether, and in what way, the degradation mechanism for diluted and concentrated solutions are different. The possibility of making the polymer molecules fluorescent was looked into and believed to be possible.

Attempts were made to link porous media behaviour to rheological properties that could be measured on bulk solutions. It is suggested that measuring normal forces, relaxation times, and loss and storage modulus by frequency sweeps can disclose information regarding the polymer solutions' flow behaviour in porous media. This would ease the process of screening new polymer products and reduce the number of core scale experiments needed. Several measurements on polymer solutions with different synthetic polymers, concentrations and salinities were performed, but the results are as of now not thoroughly analysed. However, a couple of preliminary discoveries were made. For one, normal forces could only be measured on concentrated polymer solutions. Secondly, it was discovered that the salt to polymer ratio during mixing and hydration of

the concentrated stock solution influenced the viscosity of the final diluted product. This was suspected from observations made earlier, where it was noticed that the concentration of the stock solution had an impact on the viscosity of the final product. In short, a solution diluted from a high concentrated stock solution where the salt/polymer ratio is lower will have a higher viscosity than if the salt/polymer ratio is higher. This was further substantiated by making diluted solutions made from stock solution in pure water, which were diluted with up-concentrated salt water (to achieve the same salinity as the samples to compare with). This made the effect even stronger. The effect also lasted when the bulk samples were stored for months, and it would be interesting to investigate if it would also have a lasting effect if a salt free polymer solution was injected into a porous media saturated with salt formation water. This could increase the EOR-potential, as lower concentration of polymer could be used for the same viscosity. Even if the effect only lasted in the injection zone, it could be beneficial, as polymers in low salinity water are less prone to mechanical degradation. It could also mitigate the need for suggested pre-flush (Sheng et al., 2015).

Another issue that should be investigated, is the hypothesis that if some mechanical degradation is inevitable, using lower molecular weight polymers to start with will yield the same in-depth mobility reduction. That is, if a polymer solution of e.g., 20 MD is planned to be used, but will inevitably (by mixing, choking, injection etc.) be degraded to 10 M Dalton, starting with a 10 M Dalton solution will not lead to degradation. As LMW products are cheaper and easier to inject, this would increase the economic potential of the process.

As polymer solutions are shear-thinning, their propagation rate will be determined by the prevailing shear rate. This is calculated from Equation (37), containing the somewhat enigmatic  $\alpha$ -factor. What value is used for the alpha-factor might not influence predictions of polymer flow in a homogenous system drastically, but if it is different for different porous media properties, it will supposedly influence prediction of how fast polymer solutions will flow in different layers of a reservoir. To investigate this, a flooding rig with parallel core holders was constructed. The plan was to inject different polymer solutions (both synthetic and biopolymers) and have cores with different properties in the two core holders. By measuring how the injection rate was distributed in the two cores, the plan was to fit the result with different  $\alpha$ -factors and see if it

### *Further work*

---

varied for different porous mediums and/or different polymer properties. If the  $\alpha$ -factors were found to differ dramatically, the plan was to find out how this was linked to porous media properties, and if successful, this new knowledge could be used to improve field scale modelling of polymer projects. This plan was inspired by Langaas and Stavland (2020)

## **6 Concluding remarks**

To briefly sum-up the key-points to take from this work:

It was confirmed that Partially hydrolyzed polyacrylamide viscosity is drastically reduced with increasing salinity, and that this effect is reduced if ATBS is incorporated into the polymer.

It was also found that mechanical degradation of HPAM is worsened with increasing salinity, whereas if ATBS is present in the polymer molecule, degradation is almost the same in sea-water-type solutions as in low salinity NaCl-solutions.

A power-law length-dependent degradation was found for linear core floods. Since this was associated with very high-pressure gradients, we argue that for a field case the velocity will have to decline with distance, and since mechanical degradation decreases with both velocity and molecular weight, there will probably not be additional mechanical degradation in-depth.

Mechanical degradation in pipe flow was found to scale with shear-rate, and not with Reynolds number, length, or velocity. Polymer solutions can thus be transported over long distances even at turbulent flow, but traditional chokes where the pressure drop is imposed over a short distance in a narrow opening will destroy traditional EOR-polymers. However, there are alternatives to traditional chokes, and three alternatives were directly identified; choking concentrated solution, taking the pressure drop out over a larger distance or by using several chokes in series.

The TAP systems investigated possess many of the favourable trades anticipated for this class of polymer; flow behaviour as a regular polymer at low temperature, high resistance to flow (high mobility reduction) in the porous media at high temperature and in-depth shear rates, and all this not only tolerant to salt, but also improved by salinity. Still, a better understanding of the polymer/polymer and polymer/porous media interactions during complex flow is needed to resolve challenges regarding the response time and the breakdown of the associative resistance to flow at very low shear rate.

As of today, it is hard to identify what are the main challenges thwarting the implementation of polymer EOR on the NCS. In the current low oil price scenario, economic considerations are of course important. Political signals regarding the lifetime of the industry, will certainly also make it difficult for the companies to make the necessary investments to prepare the installations for handling and preparing polymer solutions and polymer waste, which will ultimately be produced. In addition, Norway has one of the strictest environmental legislations in the world, limiting the use of biopolymers, as adding biocides are prohibited. Furthermore, the use of HPAM based polymers is strongly restricting. On the other hand, continued research on improved oil recovery, including polymer EOR, is strongly encouraged by the NPD. HPAM injection is currently being performed on the British sector of the North Sea, allegedly showing promising results, which regarding implementation and economics should be translatable to fields on NCS. Regarding the environmental issues, one may suggest that this should be balanced against the impact of exploration and development of new fields, and polymer flooding's beneficial impact on reduced water production. Reduced water production will reduce the energy needed to lift, rinse, and reinject potentially toxic formation water.

In my opinion, a method as proven and promising as polymer flooding deserves a field pilot offshore Norway before one can deem whether the disadvantages outweigh the benefits.

New promising polymer concepts, such as TAPs are continuously being developed and their many beneficial properties are attracting the attention of oil companies. Despite the many advantages that seems to come with hydrophobically associating polymers and especially the thermo-thickening type, few field cases are reported. An offshore pilot in the Bohain Oilfield in China is reported by Han et al. (2006), and its success was attributed to the high salt tolerance of the hydrophobically associating polymer. One reason why more field tests have not been performed could be the uncertainties related to the delayed effect of the build-up of resistance to flow (Åsen et al., 2021) and how this will play out at large scale. This should be investigated further. Other reasons could be economical; tailored stimuli responsive polymer might be expensive to develop and produce. However, production cost should decline if demands increase so that production can be scaled up.

### *Concluding remarks*

---

Based on results from this work, the recommendation for a polymer flood would be to identify all operation steps that could mechanically harm a polymer solution, remove or change as many as possible of these, and then identify and use the molecular weight and polymer type that would pass almost unharmed through the steps that can not be eliminated. If low salinity water is attainable, the positive effects of this with regards to allowing lower concentrations of cheaper polymers, reduced degradation, and possible low-salinity EOR-effects must be compared to the cost of attaining (producing or supplying) low-salinity water. Mixing the polymer solution at the low salinity water source might be an option. This will save space at the injection site, and this work has shown that polymer solution can be transported in pipes without degradation. Synthetic polymers also have a strong drag reduction ability, reducing the energy needed to transport the solution, compared to a fluid of the same viscosity. If low salinity water is not attainable at an acceptable cost, ATBS-type co-polymers should be used. If the main part of the reservoir has an elevated temperature compared to the injection zone, investing some time and resources to identify a suitable TAP, could pay off in the long run, considering the concept's many favourable properties.

## 7 References

- Amit, D. J., Parisi, G., & Peliti, L. (1983). Asymptotic behavior of the "true" self-avoiding walk. *Physical Review B*, 27(3), 1635.
- Askarinezhad, R., Universitetet i Stavanger Institutt for energi- og, p., & Universitetet i, S. (2018). *Produced water management : chemical water shutoff and disproportionate permeability reduction* University of Stavanger, Faculty of Science and Technology, Department of Petroleum Engineering]. Stavanger.
- Austad, T., Strand, S., Madland, M. V., Puntervold, T., & Korsnes, R. I. (2007). Seawater in chalk: an EOR and compaction fluid. International petroleum technology conference,
- Azad, M. S., & Trivedi, J. J. (2019). Quantification of the viscoelastic effects during polymer flooding: a critical review. *SPE Journal*, 24(06), 2,731-732,757.
- Azad, M. S., & Trivedi, J. J. (2020). Extensional Effects during Viscoelastic Polymer Flooding: Understanding Unresolved Challenges. *SPE Journal*.
- Baschnagel, J., Wittmer, J. P., & Meyer, H. (2004). Monte Carlo simulation of polymers: coarse-grained models. *arXiv preprint cond-mat/0407717*.
- Baviere, M. (1991). Basic concepts in enhanced oil recovery processes.
- Blasius, H. (1913). Das aehnlichkeitsgesetz bei reibungsvorgängen in flüssigkeiten. In *Mitteilungen über Forschungsarbeiten auf dem Gebiete des Ingenieurwesens* (pp. 1-41). Springer.
- Bokias, G., Hourdet, D., & Iliopoulos, I. (2000). Positively charged amphiphilic polymers based on poly (N-isopropylacrylamide): Phase behavior and shear-induced thickening in aqueous solution. *Macromolecules*, 33(8), 2929-2935.
- Borling, D., Chan, K., Hughes, T., & Sydnask, R. (1994). Pushing out the oil with conformance control. *Oilfield Review;(Netherlands)*, 6(2).
- Cannella, W., Huh, C., & Seright, R. (1988). Prediction of xanthan rheology in porous media. SPE annual technical conference and exhibition,
- Carman, P. C. (1956). Flow of gases through porous media.  
[Record #67 is using a reference type undefined in this output style.]
- Cohen, Y., & Christ, F. (1986). Polymer retention and adsorption in the flow of polymer solutions through porous media. *SPE Reservoir Engineering*, 1(02), 113-118.
- Culter, J. D., Zakin, J. L., & Patterson, G. K. (1975). Mechanical degradation of dilute solutions of high polymers in capillary tube flow. *Journal of Applied Polymer Science*, 19(12), 3235-3240.

- Du, H., Wickramasinghe, R., & Qian, X. (2010). Effects of salt on the lower critical solution temperature of poly (N-isopropylacrylamide). *The Journal of Physical Chemistry B*, 114(49), 16594-16604.
- Dupuis, G., Rousseau, D., Tabary, R., & Grassl, B. (2011). Flow of hydrophobically modified water-soluble-polymer solutions in porous media: New experimental insights in the diluted regime. *SPE Journal*, 16(01), 43-54.
- Durand, A., & Hourdet, D. (1999). Synthesis and thermoassociative properties in aqueous solution of graft copolymers containing poly (N-isopropylacrylamide) side chains. *Polymer*, 40(17), 4941-4951.
- Durand, A., & Hourdet, D. (2000). Thermoassociative graft copolymers based on poly (N-isopropylacrylamide): Relation between the chemical structure and the rheological properties. *Macromolecular Chemistry and Physics*, 201(8), 858-868.
- Emadi, A. (2012). *Enhanced heavy oil recovery by water and carbon dioxide flood* Heriot-Watt University Edinburgh, UK].
- Fathi, S. J., Austad, T., & Strand, S. (2012). Water-Based Enhanced Oil Recovery EOR by Smart Water in Carbonate Reservoirs. SPE EOR conference at oil and gas West Asia,
- Fjelde, I., Asen, S. M., & Omekeh, A. V. (2012). Low salinity water flooding experiments and interpretation by simulations. SPE improved oil recovery symposium,
- Fjelde, I., Omekeh, A. V., & Sokama-Neuyam, Y. A. (2014). Low salinity water flooding: Effect of crude oil composition. SPE Improved Oil Recovery Symposium,
- Freed, K. F. (1981). Polymers as self-avoiding walks. *The Annals of Probability*, 537-554.
- Gathier, F., Christophe, R., Lionel, L., & Antoine, T. (2020). Offshore Polymer EOR Injection Philosophies, Constrains and Solutions. SPE Improved Oil Recovery Conference,
- Han, M., Xiang, W., Zhang, J., Jiang, W., & Sun, F. (2006). Application of EOR technology by means of polymer flooding in Bohai Oilfields. International Oil & Gas Conference and Exhibition in China,
- Hirasaki, G., & Pope, G. (1974). Analysis of factors influencing mobility and adsorption in the flow of polymer solution through porous media. *Society of Petroleum Engineers Journal*, 14(04), 337-346.
- Hourdet, D., L'alloret, F., & Audebert, R. (1994). Reversible thermo-thickening of aqueous polymer solutions. *Polymer*, 35(12), 2624-2630.
- Israelachvili, J. N. (2011). *Intermolecular and surface forces*. Academic press.
- Jensen, T., Harpole, K., & Østhus, A. (2000). EOR screening for Ekofisk. SPE European Petroleum Conference,

## References

---

- Jolma, I., Strand, D., Stavland, A., Fjelde, I., & Hatzignatiou, D. (2017). When size matters-polymer injectivity in chalk matrix. IOR 2017-19th European Symposium on Improved Oil Recovery,
- Jouenne, S., Anfray, J., Levitt, D., Souilem, I., Marchal, P., Lemaitre, C., Choplin, L., Nesvik, J., & Waldman, T. (2015). Degradation (or lack thereof) and drag reduction of HPAM solutions during transport in turbulent flow in pipelines. *Oil and gas facilities*, 4(01), 80-92.
- Jouenne, S., Chakibi, H., & Levitt, D. (2018). Polymer stability after successive mechanical-degradation events. *SPE Journal*, 23(01), 18-33.
- Kamal, M. S., Sultan, A. S., Al-Mubaiyedh, U. A., & Hussein, I. A. (2015). Review on polymer flooding: rheology, adsorption, stability, and field applications of various polymer systems. *Polymer Reviews*, 55(3), 491-530.
- Karami, H. R., Rahimi, M., & Ovaysi, S. (2018). Degradation of drag reducing polymers in aqueous solutions. *Korean Journal of Chemical Engineering*, 35(1), 34-43.
- Kim, C., Kim, J., Lee, K., Choi, H., & Jhon, M. (2000). Mechanical degradation of dilute polymer solutions under turbulent flow. *Polymer*, 41(21), 7611-7615.
- Kim, U., & Carty, W. M. (2016). Effect of polymer molecular weight on adsorption and suspension rheology. *Journal of the Ceramic Society of Japan*, 124(4), 484-488.
- Kozeny, J. (1927). Über kapillare leitung der wasser in boden. *Royal Academy of Science, Vienna, Proc. Class I*, 136, 271-306.
- Kronberg, B., Holmberg, K., & Lindman, B. (2014). *Surface chemistry of surfactants and polymers*. John Wiley & Sons.
- Kruschwitz, S., Halisch, M., Prinz, C., Weller, A., Müller-Petke, M., & Dlugosch, R. (2017). Towards a better understanding of electrical relaxation. Annual Symposium of the Society of Core Analysts (SCA) Proceedings,
- Kwak, H. T., Zhang, G., & Chen, S. (2005). The effects of salt type and salinity on formation water viscosity and NMR responses. proceedings of the international symposium of the Society of Core Analysts, Toronto, Canada,
- L'alloret, F., Maroy, P., Hourdet, D., & Audebert, R. (1997). Reversible thermoassociation of water-soluble polymers. *Revue de l'Institut Français du Pétrole*, 52(2), 117-128.
- Langaas, K., & Stavland, A. (2020). Water Shutoff with Polymer in the Alvheim Field. *SPE Production & Operations*, 35(02), 335-350.
- Lara-Ceniceros, T. E., Cadenas-Pliego, G., Rivera-Vallejo, C. C., de León-Gómez, R. E. D., Coronado, A., & Jiménez-Regalado, E. J. (2014).

- Synthesis and characterization of thermo-insensitive, water-soluble associative polymers with good thickening properties at low and high temperatures. *Journal of Polymer Research*, 21(7), 1-12.
- Leblanc, T., Braun, O., Thomas, A., Divers, T., Gaillard, N., & Favero, C. (2015). Rheological properties of stimuli-responsive polymers in solution to improve the salinity and temperature performances of polymer-based chemical enhanced oil recovery technologies. SPE Asia Pacific Enhanced Oil Recovery Conference,
- Lohne, A., Nødland, O., Stavland, A., & Hiorth, A. (2017). A model for non-Newtonian flow in porous media at different flow regimes. *Computational Geosciences*, 21(5), 1289-1312.
- Maerker, J. M. (1975). Shear degradation of partially hydrolyzed polyacrylamide solutions. *Society of Petroleum Engineers Journal*, 15(04), 311-322.
- Maloney, D., Honarpour, M., & Brinkmeyer, A. (1990). *The effects of rock characteristics on relative permeability*.
- Manrique, E., Ahmadi, M., & Samani, S. (2017). Historical and recent observations in polymer floods: an update review. *CT&F Ciencia, Tecnología y Futuro*, 6(5), 17-47.
- Martin, F. (1986). Mechanical degradation of polyacrylamide solutions in core plugs from several carbonate reservoirs. *SPE Formation Evaluation*, 1(02), 139-150.
- Muggeridge, A., Cockin, A., Webb, K., Frampton, H., Collins, I., Moulds, T., & Salino, P. (2014). Recovery rates, enhanced oil recovery and technological limits. *Philosophical Transactions of the Royal Society A: Mathematical, Physical and Engineering Sciences*, 372(2006), 20120320.
- NorwegianPetroleum. (2019). The government's revenues. URL: <https://www.norskpetroleum.no/en/economy/governments-revenues>.
- Nouri, H. H., & Root, P. J. (1971). A study of polymer solution rheology, flow behavior, and oil displacement processes. Fall Meeting of the Society of Petroleum Engineers of AIME,
- NPD. (2019). NPD. Retrieved 31.01.2021 from <https://factpages.npd.no/en/field/pageview/all/26376286>
- Nødland, O., Lohne, A., Stavland, A., & Hiorth, A. (2019). An investigation of polymer mechanical degradation in radial well geometry. *Transport in Porous Media*, 128(1), 1-27.
- Nødland, O. M. (2019). *Core scale modelling of EOR transport mechanisms* [University of Stavanger, Faculty of Science and Technology, Department of Mathematics and Natural Sciences]. Stavanger, Norway.

## References

---

- Palmer, T. L., Baardsen, G., & Skartlien, R. (2018). Reduction of the effective shear viscosity in polymer solutions due to crossflow migration in microchannels: Effective viscosity models based on DPD simulations. *Journal of Dispersion Science and Technology*, 39(2), 190-206.
- Piñerez T, I. D., Austad, T., Strand, S., Puntervold, T., Wrobel, S., & Hamon, G. (2016). Linking low salinity EOR effects in sandstone to pH, mineral properties and water composition. SPE Improved Oil Recovery Conference,
- Polymer Properties Database* (2015-2016).  
<https://polymerdatabase.com/polymer%20physics/Molecular%20Weight.html#:~:text=It%20is%20a%20measure%20for,broader%20the%20molecular%20weight%20distribution.&text=where%20%5B%CE%20%5D%20is%20the%20intrinsic,been%20measured%20for%20many%20polymers>
- Poole, R. (2012). The Deborah and Weissenberg numbers. *Rheol. Bull.*, 53(2), 32-39.
- Pye, D. J. (1964). Improved secondary recovery by control of water mobility. *Journal of Petroleum Technology*, 16(08), 911-916.
- Reichenbach-Klinke, R., Stavland, A., Langlotz, B., Wenzke, B., & Brodt, G. (2013). New insights into the mechanism of mobility reduction by associative type copolymers. SPE Enhanced Oil Recovery Conference,
- Reichenbach-Klinke, R., Stavland, A., Strand, D., Langlotz, B., & Brodt, G. (2016). Can associative polymers reduce the residual oil saturation? SPE EOR Conference at Oil and Gas West Asia,
- Reichenbach-Klinke, R., Zimmermann, T., Stavland, A., & Strand, D. (2018). Temperature-Switchable Polymers for Improved Oil Recovery. SPE Norway One Day Seminar,
- Reiner, M. (1964). The Deborah number. *Physics Today*, 17(1), 62.
- Ritchie, H. (2020). *Energy mix*. Retrieved 12.01.2021 from <https://ourworldindata.org/energy-mix>
- Ruiz-Cañas, M.-C., Quintero-Perez, H.-I., Castro-García, R.-H., & Romero-Bohorquez, A. R. (2020). USE OF NANOPARTICLES TO IMPROVE THERMOCHEMICAL RESISTANCE OF SYNTHETIC POLYMER TO ENHANCED OIL RECOVERY APPLICATIONS: A REVIEW. *CT&F-Ciencia, Tecnología y Futuro*, 10(2), 85-97.
- Ryles, R. (1988). Chemical stability limits of water-soluble polymers used in oil recovery processes. *SPE Reservoir Engineering*, 3(01), 23-34.
- Sachdeva, J. S., Nermoen, A., Korsnes, R. I., & Madland, M. V. (2020). Effect of Initial Wettability on Rock Mechanics and Oil Recovery: Comparative Study on Outcrop Chalks. *Transport in Porous Media*, 133(1), 85-117.

## References

---

- Seright, R., & Skjevrak, I. (2015). Effect of dissolved iron and oxygen on stability of hydrolyzed polyacrylamide polymers. *SPE Journal*, 20(03), 433-441.
- Seright, R. S. (1983). The effects of mechanical degradation and viscoelastic behavior on injectivity of polyacrylamide solutions. *Society of Petroleum Engineers Journal*, 23(03), 475-485.
- Seright, R. S., Fan, T., Wavrik, K., & de Carvalho Balaban, R. (2011). New insights into polymer rheology in porous media. *SPE Journal*, 16(01), 35-42.
- Sheng, J. J., Leonhardt, B., & Azri, N. (2015). Status of polymer-flooding technology. *Journal of Canadian petroleum technology*, 54(02), 116-126.
- Skrettingland, K., Dale, E. I., Stenerud, V. R., Lambertsen, A. M., Nordaas Kulkarni, K., Fevang, O., & Stavland, A. (2014). Snorre In-depth Water Diversion Using Sodium Silicate-Large Scale Interwell Field Pilot. SPE EOR Conference at Oil and Gas West Asia,
- Skrettingland, K., Holt, T., Tweheyo, M. T., & Skjevrak, I. (2011). Snorre low-salinity-water injection—coreflooding experiments and single-well field pilot. *SPE Reservoir Evaluation & Engineering*, 14(02), 182-192.
- Smalley, P., Muggeridge, A., Dalland, M., Helvig, O., Høgnesen, E., Hetland, M., & Østhus, A. (2018). Screening for EOR and Estimating Potential Incremental Oil Recovery on the Norwegian Continental Shelf. SPE Improved Oil Recovery Conference,
- Sorbie, K. (1991). Polymer-improved oil recovery.
- Standnes, D. C., & Skjevrak, I. (2014). Literature review of implemented polymer field projects. *Journal of Petroleum Science and Engineering*, 122, 761-775.
- Stavland, A., Jonsbraten, H., Lohne, A., Moen, A., & Giske, N. H. (2010). Polymer flooding-flow properties in porous media versus rheological parameters. SPE EUROPEC/EAGE Annual Conference and Exhibition,
- Stavland, A., & Nilsson, S. (2001). Segregated flow is the governing mechanism of disproportionate permeability reduction in water and gas shutoff. SPE annual technical conference and exhibition,
- Stavland, A., Åsen, S. M., Mebratu, A., & Gathier, F. (2021). Scaling of Mechanical Degradation of EOR Polymers: From Field-Scale Chokes to Capillary Tubes. *SPE Production & Operations*, 36(01), 43-56.
- Szabo, M. T. (1975). Some aspects of polymer retention in porous media using a C14-tagged hydrolyzed polyacrylamide. *Society of Petroleum Engineers Journal*, 15(04), 323-337.

- Taylor, K. C., & Nasr-El-Din, H. A. (1998). Water-soluble hydrophobically associating polymers for improved oil recovery: A literature review. *Journal of Petroleum Science and Engineering*, 19(3-4), 265-280.
- Teeuw, D., & Hesselink, F. T. (1980). Power-law flow and hydrodynamic behaviour of biopolymer solutions in porous media. SPE Oilfield and Geothermal Chemistry Symposium,
- Warner, H. (1976). Analysis of mechanical degradation data on partially hydrolyzed polyacrylamide solutions. *SPE J.*
- Weast, R. C., & Astle, M. (1983). *CRC Handbook of Chemistry and Physics* (63 ed.).
- Zaitoun, A., & Kohler, N. (1987). The role of adsorption in polymer propagation through reservoir rocks. SPE International Symposium on Oilfield Chemistry,
- Zaitoun, A., Makakou, P., Blin, N., Al-Maamari, R. S., Al-Hashmi, A., Abdel-Goad, M., & Al-Sharji, H. H. (2012). Shear stability of EOR polymers. *SPE Journal*, 17(02), 335-339.
- Zhang, G., & Seright, R. (2014). Effect of concentration on HPAM retention in porous media. *SPE Journal*, 19(03), 373-380.
- Zheng, C., Gall, B., Gao, H., Miller, A., & Bryant, R. (2000). Effects of polymer adsorption and flow behavior on two-phase flow in porous media. *SPE Reservoir Evaluation & Engineering*, 3(03), 216-223.
- Zhong, C., Luo, P., Ye, Z., & Chen, H. (2009). Characterization and solution properties of a novel water-soluble terpolymer for enhanced oil recovery. *Polymer Bulletin*, 62(1), 79-89.
- Zhu, Y., Xu, Y., & Huang, G. (2013). Synthesis and aqueous solution properties of novel thermosensitive polyacrylamide derivatives. *Journal of Applied Polymer Science*, 130(2), 766-775.
- Åm, K., Al-Kasim, F., Bjerkedal, N., Gjerdseth, A., Kindem, S., Skauge, A., Skjaerpe, T., Sund, B., Saetre, J., & Wiborg, R. (2010). Oekt utvinning paa norsk kontinentalsokkel-en rapport fra utvinningsutvalget. *Olje-og energidepartementet, Oslo.*
- Åsen, S. M., Stavland, A., & Strand, D. (2021). Flow behavior of thermo-thickening associative polymers in porous media: Effects of associative content, salinity, time, velocity, and temperature. *Submitted to Transport in Porous Media.*
- Åsen, S. M., Stavland, A., Strand, D., & Hiorth, A. (2018). An experimental investigation of polymer mechanical degradation at cm and m scale. SPE Improved Oil Recovery Conference,
- Åsen, S. M., Stavland, A., Strand, D., & Hiorth, A. (2019). An Experimental Investigation of Polymer Mechanical Degradation at the Centimeter and Meter Scale. *SPE Journal*, 24(04), 1,700-701,713.

---

## PAPERS

Unfortunately, due to copyright restrictions, the papers cannot be included in Brage.

They are:

Journal paper 1:

Åsen, S. M., Stavland, A., Strand, D., & Hiorth, A. (2019). An Experimental Investigation of Polymer Mechanical Degradation at the Centimeter and Meter Scale. *SPE Journal*, 24(04), 1-700. SPE-190225-PA (Åsen et al., 2019). <https://doi.org/10.2118/190225-PA>

Journal paper 2:

Stavland, A., Åsen, S. M., Mebratu, A., & Gathier, F. (2020). Scaling of Mechanical Degradation of EOR-polymers: From Field-Scale Chokes to Capillary Tubes. *SPE Production & Operations*. SPE-202478-PA (Stavland et al., 2021). <https://doi.org/10.2118/202478-PA>

Journal paper 3 (submitted):

Åsen, S. M., Stavland, A., & Strand, D. (submitted, March 2021). Flow behavior of thermo-thickening associative polymers in porous media: Effects of associative content, salinity, time, velocity, and temperature. Submitted to *Transport in Porous Media* (Åsen et al., 2021).